INVESTIGATION OF SODIUM BINDING THROUGH IMPLEMENTATION AND APPLICATION OF SINGLE- AND DOUBLE-QUANTUM FILTERED ^{23}NA NMR SPECTROSCOPY

BY

EMILY DEFNET

THESIS

Submitted in partial fulfillment of the requirements
for the degree of Master of Science in Food Science and Human Nutrition
with a concentration in Food Science
in the Graduate College of the
University of Illinois at Urbana-Champaign, 2015

Urbana, Illinois

Adviser:

Professor Shelly J. Schmidt

ABSTRACT

Reduction of sodium in foods is a top priority in today's food industry. However, sodium removal, due to its vital importance as a tastant, as well as its contribution to many other food properties, is no simple task. A method that would measure sodium ion mobility and correlate to saltiness perception would be of great value. ^{23}Na NMR spectroscopy is such a method, since it offers a unique means for non-invasively measuring both sodium content and mobility using recently developed single-quantum (SQ) and double-quantum filtered (DQF) NMR experiments.

In food products, sodium ions exist in two environments – free (unassociated) and bound (associated). Free sodium ions are mobile in the aqueous phase, whereas bound sodium ions are associated with negatively charged functional groups in the system, such as amine and carboxyl groups associated with protein and carbohydrate macromolecules. The SQ NMR experiment provides information regarding the total sodium ion population in the system, while the DQF experiment specifically focuses on the population of bound sodium ions. Recently, the concentration of free sodium ions, measured using the ^{23}Na NMR SQ-DQF methods, was shown to strongly correlate to saltiness perception in cheeses. Therefore, it is important to investigate sodium ion binding, using a relative ratio of bound to total sodium, in specific food systems, and how that binding changes as a function of sodium ion addition and removal from the matrix. However, the SQ and DQF ^{23}Na NMR methods have never before been established here at the University of Illinois at Urbana-Champaign.

Thus, the first objective of this study was to implement the ^{23}Na NMR methods using a 1% (w/w) iota-carrageenan system and verify the method with previously published literature data. The second objective was to apply the ^{23}Na NMR SQ and DQF methods to

both reduced-fat (30%) and low-fat (20%) model emulsion systems, meant to model a ranch salad dressing, containing water, oil, soy lecithin, xanthan gum, and NaCl, where added sodium concentrations ranged from 0 to 350mg per 30g serving. Two fat levels were studied since differences in fat content have been shown to have varying effects on saltiness perception.

The SQ and DQF ^{23}Na NMR methods were effectively implemented and verified using an iota-carrageenan system. In addition, the relative quantification of bound to total sodium was determined for the model emulsions, and correlations were investigated between sodium mobility (T_1 and T_2), sodium binding (A_{DQ}/A_{SQ}), viscosity, and pH. It was found that the ratio of bound to total sodium (A_{DQ}/A_{SQ}) remained constant for the reduced-fat formulations, but decreased for the low-fat formulations, indicating the potential of more free sodium in the low-fat versions. It was also found that the reduced-fat formulations had a higher viscosity than the low-fat emulsions, which could contribute to the need for more added sodium in the higher fat formulations. With a greater understanding of the effect of sodium binding on saltiness perception in specific food systems, those systems can be more efficiently engineered to maximize saltiness perception, while containing the least amount of sodium possible.

ACKNOWLEDGEMENTS

This thesis would not have been possible without the help and support of many people. First and foremost, I would like to thank my advisor, Dr. Shelly Schmidt, for her guidance and wisdom over the past two years. Her constant encouragement and support has motivated me to work to my full potential and to pursue my goals. I would also like to thank the other members of my thesis committee, Dr. Soo-Yeun Lee and Dr. Youngsoo Lee, for their suggestions along the way to help direct and shape this work into its final form.

Dr. Lingyang Zhu, from the NMR Lab of the School of Chemical Sciences, was instrumental in the NMR portion of this research. I am very grateful for her support, guidance, and dedication to this project. I would also like to extend much appreciation to Ginnefer Cox, for her emulsion formulation and sensory, pH, and viscosity data. Her work and wisdom were extremely helpful.

My labmates deserve many thanks for their support, wisdom, guidance, and help in keeping me sane. It was a privilege to work with such a kind, caring, and fun group of people, and I am honored to call them my friends.

Finally, I would like to thank my family and friends for their love, support, and faith in me to complete this journey. They have been there for me in every step of my academic career, and always encouraged me to pursue my passions – and for that, I am extremely grateful.

Table of Contents

Chapter 1: Literature Review

1.1 Introduction

Excessive intake of sodium is a major problem facing the United States and the world today. Overconsumption of sodium has been shown to cause an increased risk of high blood pressure, stroke, poor bone health, kidney disease, and stomach cancer (Kim and others 2012). The 2010 Dietary Guidelines for Americans suggests reducing sodium intake to less than 2,300 mg per day, with an even stricter recommendation of less than 1,500 mg per day for persons who are 51 and older, or those of any age who are African American or have hypertension, diabetes, or chronic kidney disease (USDA 2010). Despite these guidelines, Americans at or above the age of 2 consume an average of over 3,400 mg of sodium per day (USDA 2005-2006). Of that sodium, only a small portion is added at the table – the majority of sodium is consumed from processed foods (USDA 2005-2006). However, the direct removal of sodium from food products without replacement or other alterations would have a significant impact on many facets of the food system, including taste, microbial stability, flavor development, and texture formation, making sodium reduction a very complex and challenging problem (Kim and others 2012).

1.2 Salty Perception

1.2.1 Mechanism of Salty Taste

Sodium ions, present in foods through the dissociation of NaCl, interact with various food components and external stimuli to impact salty taste. Saltiness is due to the dissociation of ionic salts, such as NaCl, KCl, and $CaCl_2$, into their positively charged

cations and negatively charged anions. While the anion of the salt influences salty taste, saltiness is primarily a function of the Na^+ cation (Bartoshuk 1980). As depicted in Figure 1.1, specific taste receptor cells on the tongue express the epithelial sodium (Na) channel (ENaC), to which sodium ions dissolved in the saliva bind (Chandrashekar and others 2010). The sodium ions then move from outside to inside the taste receptor cell, resulting in a release of neurotransmitters that eventually cause the brain to recognize the taste as salty (McCaughey and Scott 1998).

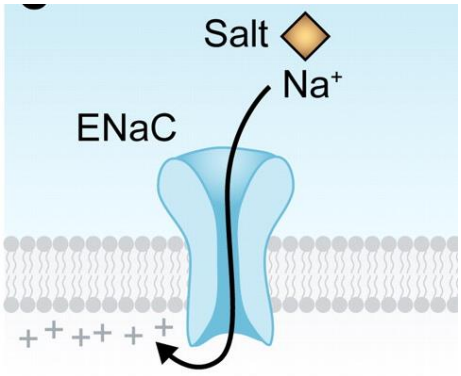

Figure 1.1. Depiction of epithelial sodium channel (ENaC) to describe the mechanism of salty taste (Excerpted from Chaudhari and Roper 2010).

1.2.2 Correlation between Fat Content and Salty Perception

There are a number of studies that have investigated the relationship between fat content and salty perception, but these studies resulted in contradictory views on the correlation between the two attributes. Some studies found that an increase in fat content led to an increase in salty perception, in products including salad cream (a mayonnaise-like dressing and spread) (Shamil and others 1991-1992), model dairy products (Panouille and others 2011), model cheeses (Phan and others 2008), cream cheese (Wendin and others 2000), and cooked bologna-type sausages (Ruusunen and others 2001). However, in each of these studies, fat content was not the only component of the

formulation that was varied. In the experiments involving the salad cream, cream cheese, model cheese, and model dairy product, the fat was replaced with water in the lower fat formulations, resulting in a lower concentration of sodium in the aqueous phase. It has been shown that higher concentrations of sodium in the aqueous phase leads to an increased salty perception; therefore, a lower concentration of sodium in the aqueous phase could contribute to a lower salty perception in lower fat products (Shamil and others 1991-1992). In the studies involving the model dairy product and cooked bologna-type sausages, fat was replaced with protein in lower fat varieties. The higher protein content could create more opportunities for sodium binding, which would result in a lower concentration of free sodium in the aqueous phase, that could result in a reduced salty perception in the higher protein/lower fat samples (Ruusunen and others 2001).

While those studies concluded that increasing fat increases saltiness perception, other experiments have found that salty perception decreases as fat content increases. In one study involving frankfurters, water replaced fat to keep the protein content consistent among samples (Hughes and others 1997), while in a separate study involving frankfurters, the protein level and water content increased as fat decreased (Paneras and others 1996). Previous authors would predict that those compensatory effects would increase salty perception in higher fat versions, but instead, a decrease in salty perception was found. This discrepancy could be due to a decreased water holding capacity in the lower-fat versions - if the water content is lower in the final product of the lower-fat versions compared to the full-fat versions, that difference could lead to an increase in NaCl concentration in the aqueous phase, and therefore an increase in saltiness in the lower-fat products. A study that investigated white-brined cheese found the full fat

version to be less salty than the lower fat variants, even though the NaCl concentration was calculated to be constant in each cheese water phase, and the protein content increased as fat content decreased (Romeih and others 2002).

Lastly, some studies reported no correlation between fat content and saltiness perception. In one study with cooked bologna-type sausages, the protein increased as fat content decreased, but the water content was held constant for all formulations (Ventanas and others 2010). In an additional study with the same product, when water was replaced with pork fat on an equal weight basis, the perceived saltiness still did not change (Ruusunen and others 2001). When a model cheese system was investigated, the quantity of bound sodium remained the same for each of the varied fat formulations (Lauverjat and others 2009). Finally, for a study involving bovine and ovine halloumi cheese, milk fat levels were adjusted to produce consistent protein:fat ratios for the reduced- and low-fat cheeses (Lteif and others 2009).

The lack of agreement on the effect of fat content on sodium perception in various food products indicates that many components and variables have an impact on salty taste, and many studies have only investigated specific aspects without considering all product components, how the sodium is released from the product, and how the sodium is available in the mouth to be perceived (Kuo and Lee 2014). It has been shown that fat, because it is a hydrophobic substance, can act as a barrier against sodium migration, and thus disfavors its release from a food matrix (Hughes and others 1997). In addition, once in the mouth, fat has been shown to coat the tongue surface, thus hindering the availability of sodium to the taste buds (Lynch and others 1993). However, other studies have shown that certain components of fat may sensitize taste receptor cells, which would

result in a higher response towards sodium (Gilbertson and others 2005). The effect of fat on salty perception is difficult to predict without taking into account all aspects of the food, sodium release from the food, and interaction between sodium and the taste receptor cells in the mouth.

1.2.3 Oil-in-Water Emulsions

When Cox and Lee (2010) investigated the correlation between sodium content and fat content in ten major processed food categories, a compensatory effect was found for selected categories. For ranch salad dressing specifically, the reduced-fat version was found to have a statistically higher concentration of sodium than its regular counterpart. This decrease in sodium content with decrease in fat content could be explained by sensory findings from experiments with oil-in-water emulsions (Yamamoto and Nakabayashi 1999; Malone and others 2003; Suzuki and others 2010). Those studies found that perceived saltiness increased with increasing oil content, presumably because of the associated increase in salt concentration in the aqueous phase as oil content increased, assuming NaCl is distributed in the water phase. However, all 3 studies found that when the concentration of salt in the aqueous phase was kept constant, and oil content was increased, the saltiness was found to decrease. These results indicate that salty perception is not simply dependent on the concentration of salt in the aqueous phase, but may also be affected by the suppressed contact of NaCl to the taste receptor cells (Yamamoto and Nakabayashi 1999). The decrease in salty taste with increasing fat content could also be attributed to the reduction in surface area of water in the sample. It has been shown that taste detection thresholds are proportional to both contact surface area and sample volume. A power law relationship between perceived intensity (I) and

surface area was (A) proposed ($I = k'A^{n'}$), where the value of n' was dependent on the type of tastant (Smith 1971). This suggests that increasing the oil phase volume of an oil-in-water emulsion would reduce the volume of water in the sample, and for a constant concentration of sodium in the aqueous phase, the perceived intensity would be expected to decrease (Malone and others 2003).

In separate investigation of oil-in-water emulsions, it was found that fat had no effect on saltiness intensity, after correcting for the NaCl concentration differences in the aqueous phase (Metcalf and Vickers 2002). However, in the studies by Malone and others (2003) and Yamamoto and Nakabayashi (1999), the oil concentration was 70% in the highest fat emulsion, whereas in the study by Metcalf and Vickers (2002), the oil content only ranged between 9 and 17%. The higher oil content in the previous studies may have created a barrier between the aqueous phase and the taste receptors (Metcalf and Vickers 2002). More studies need to be conducted to fully understand the effect of fat on salty perception in oil-in-water emulsions.

1.3. Use of ^{23}Na NMR to Measure Sodium Ion Mobility

1.3.1 Mobility of Total Sodium Ion Population

Sodium ions not only interact with taste receptors in the mouth, but they are also capable of associating with negatively charged amine and carboxyl groups in food macromolecules, such as proteins and carbohydrates. ^{23}Na Nuclear Magnetic Resonance (NMR) is one method that has been utilized to nondestructively, noninvasively measure the binding of sodium ions in a system. In the past, transverse relaxation rates (R_2 values), which are a measure of sodium ion mobility of the total sodium population, were

used to investigate the link between sodium mobility and saltiness perception in food products, such as meat (Lioutas and others 1988, Bertram and others 2005), hydrocolloid solutions (Rosett and others 1994, Rosett and others 1995), soups (Rosett and others 1996), and snow crab (Nagata and others 2000).

One study investigated the relationship between perceived saltiness and the binding of sodium ions to ionic (xanthan and kappa) and non-ionic (guar and locust bean) gum solutions (Rosett and others 1994). Previous research found that in general, Na^+ ions were less mobile in the ionic gum systems until a certain concentration was reached, at which point the mobility equalized between the ionic and non-ionic gums. (Shirley and others 1993). This equality in mobility is thought to be due to the concentration of NaCl exceeding anionic binding sites of the gum solutions. In addition, as the concentration of gums increased, the percentage of free Na^+ decreased. This phenomenon suggested that the sodium ions bind to the anionic binding sites. Rosett and others (1994) showed that ionic gums suppressed salty perception more than non-ionic gums, until R_2 values converged and perceived saltiness equalized. It was hypothesized that NMR R_2 values, a measure of sodium mobility, correlated well with salty perception – the more immobile the sodium, the less salty the taste. However, in a study that investigated the effect of thickening agents on sodium binding of soups, that correlation did not hold true in all cases (Rosett and others 1996). When comparing R_2 values between the thickening agents, it was found that sodium ions were less mobile, on average, in a soup thickened with Na-CMC compared to xanthan gum, guar gum, and locust bean gum. If there were a direct correlation between R_2 values and salty perception, this would suggest that Na-CMC samples would have a lower salty perception than the other samples; however, this

was not found to be the case, which suggests that there are more complex mechanisms at play.

1.3.2 Mobility of Bound Sodium Ion Population

More recently, it has been shown that ^{23}Na NMR can be utilized to more precisely measure the mobility and population of sodium ions in a system through the Double Quantum Filtration (DQF) pulse sequence, which was first demonstrated in a series of living tissue models (Whang and others 1994). It was later shown that DQF experiments could be utilized to determine not only total sodium, but bound sodium concentration as well (Mouaddab and others 2007). In a food system, positively charged sodium ions are attracted to negatively charged components (i.e. proteins, carbohydrates, etc.). The sodium ions are not permanently attached to the negatively charged binding sites (they are actually in rapid exchange with other sodium ions), but as a whole, sodium ions near the negatively charged components exhibit restricted mobility, which can be measured using the DQF pulse sequence. The concentration of free sodium ions in the system can be determined by taking the difference between the concentrations of total sodium ions and bound sodium ions. A number of studies have investigated the binding of sodium ions using the DQF experiment in different food matrices, the results of which are summarized in Table 1.1.

Table 1.1. Summary of ^{23}Na DQF Experiments from the Literature

System	Variable(s)	Results (Related to Sodium Binding)	Source
Semi-hard cheese	$[NaCl]_{added}$ (0.93%, 1.63%, 2.30%)	Detected the presence of bound sodium ions with DQF method Correlation found between total sodium concentration as determined by SQ signals and chloride ion concentration	Gobet and others 2009a
Iota-carrageenan gel (1% w/w)	$[NaCl]_{added}$ (11 concentrations between 0 and 3% w/w)	As concentration of $[NaCl]_{added}$ increased, gel hardness increased, sodium ion mobility decreased, sodium binding increased then leveled off after saturation of binding sites	Gobet and others 2009b
Semi-hard cheese	$[NaCl]_{added}$ (9.2 and 22.2 g/kg)	Sodium binding increased as the $[NaCl]_{added}$ increased	Gobet and others 2010
Dry-cured ham	Pressure (0.1, 300, 600, 900 MPa)	Reduced ratio of bound to total sodium as pressure increased, indicating reduced tendency of sodium binding with pressure increase	Picouet and others 2012
Model cheese	Lipid/Protein ratio (28/20, 24/24, 20/28) $[NaCl]_{added}$ (0 and 1%)	No significant differences were found between the ratios of bound to total sodium based on lipid/protein ratio or $[NaCl]_{added}$	Boisard and others 2013
Bread	Salt type (standard crystal, liquid + standard crystal, liquid, micronized crystals, large crystals, 50% encapsulated, 100% encapsulated) When NaCl added (at beginning or end of kneading cycle)	When salt was added at the beginning of the kneading cycle, the smallest concentration of bound sodium was found in liquid salted breads, followed by encapsulated salt When salt was added at the end of the kneading cycle, no significant differences in binding were found between salt types	Guojonsdottir and others 2013

Table 1.1. (cont.)

System	Variable(s)	Results (Related to Sodium Binding)	Source
Model cheese	Lipid/Protein ratio (28/20, 24/24, 20/28) $[NaCl]_{added}$ (0 and 1%)	The higher the $[NaCl]_{added}$, the higher the $[NaCl]_{free}$ The higher the lipid/protein ratio, the higher the $[NaCl]_{free}$ The higher the $[NaCl]_{free}$, the higher the salty perception (0.98 correlation)	Boisard and others 2014
Protein matrix	Protein type (gelatin, milk protein, soy protein) Protein concentration (2.5 and 9% w/w) pH (6.8 6.2 5.5)	As protein concentration increased, mobility of total sodium ions decreased and ratio of bound/total sodium ions increased Gelatin matrices displayed greatest mobility of total sodium ions and smallest amount of bound sodium Lowering the pH decreased the ratio of bound sodium and increased total sodium mobility Rheological properties had a larger effect on salty perception than sodium ionic binding and mobility As fracture stress and viscosity increased, firmness intensity increased and saltiness intensity increased	Mosca and others 2015

The earliest DQF experiments with food investigated sodium ion mobility in semi-hard cheeses of varying sodium concentrations (Gobet and others 2009a, Gobet and others 2010). The Gobet and others (2009a) study tested 3 cheeses with NaCl contents ranging from 0.93% (w/w) to 2.30% (w/w), while the Gobet and others (2010) study tested two cheeses with 9.2% (w/w) and 22.2% (w/w) NaCl. Both studies exhibited the capabilities of utilizing the DQF method to show the presence of sodium in a restricted environment. The DQF NMR method was later applied to iota-carrageenan systems, when sodium binding information was used to model the gelation mechanism in a 1% (w/w) iota-carrageenan system with eleven different added NaCl concentrations ranging from 0% (w/w) to 3% (w/w) (Gobet and others 2009b). The results showed that sodium ion mobility is directly correlated to gel hardness, and a mechanism for gelation was proposed, which include three stages. In the first stage, at low concentrations of added NaCl, carrageenan chains are in coil confirmation, and there is no bound sodium. In stage two, as the concentration of added NaCl increases, carrageenan strands adopt a double helix conformation, and the bound fraction of sodium increases. In the third stage, all of the sodium binding sites on the carrageenan are occupied (Gobet and others 2009b). The effect of high pressure processing in dry-cured ham on sodium ion mobility was also carried out using DQF NMR methods. Results indicated that high pressure treatments (300, 600, and 900 MPa) promote tighter binding of sodium ions to proteins than low pressures (0.1 MPa) (Picouet and others 2012).

The first quantification study to measure the absolute amount of free and bound sodium in a food system investigated the effect of salt crystal size and encapsulation on sodium mobility in bread, in which sodium can bind to the gluten (Guojonsdottir and others 2013). The study compared the salt distribution and mobility of breads with several different types of salt with

varying crystal size, liquid salt, or encapsulation of the salt, as well as the effect of when the salt is added to the process. It was found that using liquid salt, or adding salt at the end of the kneading cycle, led to the highest concentration of free sodium, and theoretically the highest salty perception, but sensory studies were not conducted to confirm the authors' hypothesis.

The correlation between salty perception and sodium binding via the DQF NMR method was not investigated until even more recently. The sodium ion mobility in model cheeses with varying salt contents and lipid/protein ratios was measured using multiple NMR parameters, and those parameters were correlated to saltiness perception. Six model cheese were prepared, containing three different lipid/protein ratios (28/20, 24/24, 20/28 %(w/w)) and two levels of added NaCl (0 and 1% (w/w)). It was shown that the smaller the lipid/protein ratio, and the lower the NaCl content, the stronger the microstructure of the cheeses, which led to a decreased mobility of sodium ions (Boisard 2013). When the sensory properties were investigated and NMR parameters were correlated to saltiness, the concentration of free sodium ions, as determined through DQF experiments, was shown to have the highest correlation to salty perception ($r^2 = 0.98$), as seen in Table 1.2 (Boisard and others 2014). Of the NMR parameters discussed, τ^{opt} represents the creation time, and is the optimal duration of τ that maximizes the DQF signal. T_1 is the longitudinal relaxation time. T_2 values, which are transverse relaxation times and the inverse of R_2 values, can be separated into fast and slow relaxations (T_{2f} and T_{2s}, respectively). A more in-depth explanation regarding the NMR parameters can be found in Chapter 2.

Table 1.2. Correlation between saltiness and NMR parameters (Excerpted from Boisard et al. 2014)

	Saltiness	W	[Na] free	*T*1/10	*T*2f	*T*2s	*T* opt
Saltiness	1	−0.43	0.98	0.71	0.84	0.51	0.82
W	−0.43	1	−0.28	−0.93	−0.81	−0.98	−0.84
[Na] free	0.98	−0.28	1	0.60	0.76	0.39	0.73
*T*1/10	0.71	−0.93	0.60	1	0.96	0.97	0.98
*T*2f	0.84	−0.81	0.76	0.96	1	0.877	0.99
*T*2s	0.51	−0.98	0.39	0.97	0.87	1	0.90
T opt	0.82	−0.84	0.73	0.99	0.99	0.907	1
C5	0.82	−0.79	0.71	0.89	0.89	0.78	0.89
C15	0.97	−0.51	0.95	0.79	0.91	0.62	0.89
C30	0.95	−0.66	0.88	0.87	0.953	0.72	0.94
Cbs	0.97	−0.48	0.94	0.75	0.89	0.57	0.86

Very recently, research has indicated that for a protein matrix system, rheological properties of a food matrix (fracture properties, viscosity) had a larger impact on salty perception than sodium mobility or binding (Mosca and others 2015). In a protein matrix in which the type of protein (gelatin, milk protein, and soy protein), concentration of protein (2.5% and 9% w/w), and pH (6.8, 6.2 and 5.5) were varied, it was found that as values of fracture stress or viscosity increased, firmness intensity increased and salty perception decreased.

The objectives of this study were twofold: Firstly, we hoped to implement and verify the SQ and DQF ^{23}Na NMR methods by comparing results for a 1% (w/w) iota-carrageenan system with 0.40 M added NaCl to previously published data. Secondly, we wanted to apply the SQ and DQF NMR methods to reduced-fat (30% fat) and a low-fat (20% fat) model emulsion systems, and investigate the relationship between sodium binding, sodium mobility, viscosity, pH, and salty perception in those systems.

1.4 References

Bartoshuk LM. 1980. Sensory analysis of the taste of NaCl. In: Kare MR, Fregly MJ, Bernard RA, eds. Biological and behavioral aspects of salt intake. New York: Academic Press. p 83-98.

Bertram HL, Holdsworth SJ, Whittaker AK, Andersen HJ. 2005. Salt diffusion and distribution in meat studied by ^{23}Na Nuclear Magnetic Resonance imaging and relaxometry. Journal of Agricultural and Food Chemistry 53(20):7814-7818.

Boisard L, Andriot I, Arnould C, Achilleos C, Salles C, Guichard E. 2013. Structure and composition of model cheeses influence sodium NMR mobility, kinetics of sodium release and sodium partition coefficients. Food Chemistry 136:1070-1077.

Boisard L, Andriot I, Martin C, Septier C, Boissard V, Salles C, Guichard E. 2014. The salt and lipid composition of model cheeses modifies in-mouth flavour release and perception related to the free sodium ion content. Food Chemistry 145:437-444.

Chandrashekar J, Kuhn C, Oka Y, Yarmolinski DA, Hummler E, Ryba NJP, Zuker CS. 2010. The cells and peripheral representation of sodium taste in mice. Nature 464(7286):297-301.

Chaudhari N and Roper SD. 2010. The cell biology of taste. Journal of Cell Biology 190(3):285-293.

Cox GO and Lee SY. 2015. Unpublished data. University of Illinois at Urbana-Champaign. Urbana, IL.

Gobet M, Foucat L, Moreau C. 2009a. Investigation of sodium ions in cheeses by ^{23}Na NMR spectroscopy. In: Guojonsdottir M, Belton P, Webb G, eds. Magnetic Resonance in Food Science: Challenges in a Changing World. Cambridge, England:Royal Society of Chemistry p 57-64.

Gobet M, Mouaddab M, Cayot N, Bonny J-M, Guichard E, Le Quere J-L, Moreau C, Foucat L. 2009b. The effect of salt content on the structure of iota-carrageenan systems: ^{23}Na DQF NMR and rheological studies. Magnetic Resonance in Chemistry 47:307-312.

Gobet M, Rondeau-Mouro C, Buchin S, Le Quere J-L, Guichard E, Foucat L, Moreau C. 2010. Distribution and mobility of phosphates and sodium ions in cheese by solid-state ^{31}P and double-quantum filtered ^{23}Na NMR spectroscopy. Magnetic Resonance in Chemistry 48:297-303.

Guojonsdottir M, Traore A, Renou JP. 2013. The effect of crystal size and encapsulation of salt on sodium distribution and mobility in bread as studied with ^{23}Na Double Quantum Filtering NMR. In: van Duynhoven J, Belton PS, Webb GA, van As H, eds. Magnetic Resonance in Food Science: Food for Thought. Cambridge, England: Royal Society of Chemistry p 35-43.

Hughes E, Cofrades S, Troy DJ. 1997. Effects of fat level, oat fibre, and carrageenan on frankfurters formulated with 5, 12, and 30% fat. Meat Science 45(3):273-281.

Kim MK, Lopetcharat K, Gerard PD, Drake MA. 2012. Consumer awareness of salt and sodium reduction and sodium labeling. Journal of Food Science 77(9):S307-13.

Kuo W-Y, Lee Y. 2014. Effect of food matrix on saltiness perception – implications for sodium reduction. Comprehensive Reviews in Food Science and Food Safety 13:906-923.

Lauverjat C, Deleris I, Trelea IC, Salles C, Souchon I. 2009. Salt and aroma compound release in model cheeses in relation to their mobility. Journal of Agricultural and Food Chemistry 57(21):9878-9887.

Lioutas TS, Baianu IC, Bechtel PJ, Steinberg MP. 1988. Oxygen-17 and Sodium-23 Nuclear Magnetic Resonance studies of myofibrillar protein interactions with water and electrolytes in relation to sorption isotherms. Journal of Agricultural and Food Chemistry 36(3):437-444.

Lteif L, Olabi A, Baghdadi OK, Toufeli I. 2009. The characterization of the physicochemical and sensory properties of full-fat, reduced-fat, and low-fat ovine and bovine halloumi. Journal of Dairy Science 92(9):4135-4145.

Malone ME, Appelqvist IAM, Norton IT. 2003. Oral behavior of food hydrocolloids and emulsions. Part 2. Taste and aroma release. Food Hydrocolloids 17(6):775-784.

McCaughey SA, Scott TR. 1998. The taste of sodium. Neuroscience and Biobehavioral Reviews 22(5):663-676.

Metcalf KL, Vickers ZM. 2002. Taste intensities of oil-in-water emulsions with varying fat content. Journal of Sensory Studies 17:379-390.

Mosca AC, Andriot I, Guichard E, Christian S. 2015. Binding of Na^+ ions to proteins: Effect on taste perception. Food Hydrocolloids 51:33-40.

Mouaddab M, Foucat L, Donnat JP, Renou JP, Bonny JM. 2007. Absolute quantification of Na^+ bound fraction by double-quantum filtered ^{23}Na NMR spectroscopy. Journal of Magnetic Resonance 189:151-155.

Nagata T, Chuda Y, Yan X, Suzuki M, Kawasaki K. 2000. The state analysis of NaCl in snow crab (Chionoecetes japonicus) meat examined by ^{23}Na and ^{35}Cl Nuclear Magnetic Resonance (NMR) spectroscopy. Journal of the Science of Food and Agriculture 80:1151-1154.

Paneras ED, Bloukas JG, Papadima SN. 1996. Effect of meat source and fat level on processing and quality characteristics of frankfurters. Lebensmittel-Wissenschaft and Technologie 29(5-6):507-514.

Panouille M, Saint-Eve A, deLoubens C, Deleris I, Souchon I. 2011. Understanding the influence of composition, structure and texture on salty perception in model dairy products. Food Hydrocolloids 25(4):716-723.

Phan VA, Yven C, Lawrence G, Chabanet C, Reparet JM, Salles C. 2008. In vivo sodium release related to salty perception during eating model cheeses of different textures. International Dairy Journal 18(9):956-963.

Picouet PA, Sala X, Garcia-Gil N, Nolis P, Colleo M, Parella T, Arnau J. 2012. High pressure processing of dry-cured ham: Ultrastructural and molecular changes affecting sodium and water dynamics. Innovative Food Science and Emerging Technologies 16:335-340.

Romeih EA, Michaelidou A, Biliaderis CG, Zerfirides GK. 2002. Low-fat white-brined cheese made from bovine milk and two commercial fat mimetics: chemical, physical and sensory attributes. International Dairy Journal 12:525-540.

Rosett TR, Shirley L, Schmidt SJ, Klein BP. 1994. Na^+ binding as measured by ^{23}Na Nuclear Magnetic Resonance spectroscopy influences the perception of saltiness in gum solutions. Journal of Food Science 59(1):206-210.

Rosett TR, Wu Z, Schmidt SJ, Ennis DM, Klein BP. 1995. KCl, $CaCl_2$, Na^+ binding and salt taste of gum systems. Journal of Food Science 60(4):849-853.

Rosett TR, Kendregan SL, Gao Y, Schmidt SJ, Klein BP. 1996. Thickening agents effects on sodium binding and other taste qualities of soup systems. Journal of Food Science 61(5):1099-1104.

Ruusunen M, Simolin M, Puolanne E. 2000. The effect of fat content and flavor enhancers on the perceived saltiness of cooked ‘bologna-type- sausages. Journal of Muscle Foods 12:107-120.

Shamil S, Wyeth LJ, Kilcast D. 1991/1992. Flavour release and perception in reduced-fat foods. Food Quality and Preference 3:51-60.

Shirley LL, Schmidt SJ. 1993. ^{23}Na NMR molecular mobility studies of hydrocolloid-NaCl solutions as influenced by sodium concentration. Food Hydrocolloids 7(2):147-156.

Smith, DV. 1971. Taste intensity as a function of area and concentration: differentiation between compounds. Journal of Experimental Psychology 87:163-171.

Stampanoni C, Noble A. 1991. The influence of fat, acid, and salt on the temporal perception of firmness, saltiness, and sourness of cheese analogs. Journal of Textural Studies 22(4):381-392.

Suzuki AH, Zhong H, Lee J, Martini S. 2014. Effect of lipid content on saltiness perception: A psychophysical study. Journal of Sensory Studies 29:404-412.

United States Department of Agriculture. 2010. Dietary Guidelines for Americans. www.dietaryguidelines.gov

U.S. Department of Agriculture, Agricultural Research Service and U.S. Department of Health and Human Services, Centers for Disease Control and Prevention. What We Eat In America, NHANES 2005–2006. http://www.ars.usda.gov/Services/docs.htm?docid=13793. Accessed April 28, 2015.

Ventanas S, Puolanne E, Tuorila H. 2010. Temporal changes of flavour and texture in cooked bologna type sausages as affected by fat and salt content. Meat Science 85(3):410-419.

Wendin K, Langton M, Caous L, Hall G. 2000. Dynamic analyses of sensory and microstructural properties of cream cheese. Food Chemistry 71(3):363-378.

Whang J, Katz J, Boxt LM, Reagan K, Sorce DJ, Sciacca RR, Cannon PJ. 1994. Multiple-Quantum-Filtered NMR determination of equilibrium magnetization for ^{23}Na quantitation in model phantoms. Journal of Magnetic Resonance, Series B 103:175-179.

Yamamoto Y, Nakabayashi M. 1999. Enhancing effect of an oil phase on sensory intensity of salt taste of NaCl in oil/water emulsions. Journal of Texture Studies 30:581-590.

Chapter 2: Implementation and Verification of the ^{23}Na SQ and DQF NMR Methods Using an Iota-carrageenan System

2.1 Introduction

^{23}Na Nuclear Magnetic Resonance (NMR) is a non-destructive, non-invasive method to determine the behavior of sodium ions in a system. There are many different pulse sequences that can elucidate different information about the sample. The single quantum (SQ) pulse sequence can be utilized to determine the total amount of sodium in a sample. However, in a food system, not all sodium ions exist in the same environment – some remain free (or unassociated), while others can bind, (or associate) with negatively charged amine and carboxyl groups in food macromolecules, such as proteins and carbohydrates. When the sodium ions interact with these negatively charged groups, they exhibit restricted mobility, which can be measured using the double quantum-filtered (DQF) pulse sequence. It has very recently been shown that the concentration of free sodium ions, which can be found by subtracting the amount of bound sodium from the total sodium, is strongly correlated with salty taste (Boisard and others 2014). In order to collect data regarding the bound sodium ions, it was necessary to implement the DQF NMR pulse sequence at the University of Illinois at Urbana-Champaign (UIUC), which has never been done before on this campus.

Therefore, the purpose of this study was to implement the SQ and DQF pulse sequences using the UI600 NMR at UIUC, and then compare the data to previously published experiments investigating sodium binding in a 1% (w/w) iota-carrageenan system with 0.4 M added NaCl in order to verify the accuracy of the method with this specific NMR instrument. In order to verify the method, first a reference was used to ensure the NMR was detecting the total sodium ion population. Then we compared reported ^{23}Na NMR parameters (T_1, A_{DQ}/A_{SQ}, τ^{opt}) to

experimental data. Finally, the absolute concentration of bound sodium in the system was attempted to be calculated.

2.2 Theoretical Background

2.2.1 NMR Basics

To collect an NMR spectrum, the sample is placed in an NMR tube, which is placed in a strong, permanent applied magnetic field (B_0). A radiofrequency (RF), also known as B_1, pulses the sample with a magnetic field at 90° to B_0; the frequency of the pulse is tuned to the resonant (Larmor) frequency of the nuclei of interest. Before the sample is pulsed, some of the nuclei are aligned with B_0, while some are aligned against it (Figure 2.1). When B_1 is applied, some of the sodium nuclei that were initially aligned against B_0, now align with the external magnetic field (Figure 2.2). However, once the pulse is no longer applied, the magnetization of those nuclei eventually returns to equilibrium by precessing around the z-axis at the resonant frequency. The magnetization undergoes two relaxation processes as it returns to equilibrium. The first is longitudinal (spin-lattice) relaxation (T_1), which is the time constant that describes how long it takes the z-vector component of magnetization (M_z) returns to equilibrium (M_0) (Figure 2.3). The second process is transverse (spin-spin) relaxation (T_2), which is the time constant that describes how quickly the magnetization in the xy plane (M_{xy}) returns to equilibrium (Figure 2.4). As M_{xy} decays, its oscillation induces a voltage in a receiver coil that is located in the xy plane. A plot of voltage intensity versus time is produced, which is also known as free induction decay (FID). The FID is converted to the familiar spectrum through Fourier Transform (FT), which converts the time domain to the frequency domain (Figure 2.5) (Ionin and Ershov 1970; Nitz and others 2010).

2.2.2 ^{23}Na NMR Theory

Sodium is able to interact with B_0 to produce a spectrum because it has an odd number of protons and neutrons in its nucleus. This characteristic is displayed in the fact that it has a non-zero spin quantum number, I (for sodium, I = 3/2), indicating the nuclei possess a magnetic field. The strength and direction of these individual magnetic fields is described by a vector quantity known as the magnetic moment (μ_n). These magnetic moments can interact with the applied magnetic field and distribute themselves about different energy levels, the differences between which can be described by the following equation:

$$\Delta E = h\nu \qquad (1)$$

where h is Planck's constant (J*s) and ν is the resonant frequency of the sodium nuclei (s^{-1}). The total number of energy levels is equal to 2I +1; therefore, since for sodium I = 3/2, there are four possible energy levels for the sodium nuclei. The values of the energy levels can be described by the magnetic quantum number, m_l, which is the measurable component of the magnetic moment, and can assume the values of –I, -I + 1, … I-1, I. Therefore, the magnetic quantum numbers for sodium are -3/2, -1/2, 1/2, and 3/2 (Woessner 2001).

2.2.2.1 Quadrupole Effects

Sodium nuclei are not only capable of interacting with applied magnetic fields, but they can also interact with electric fields (q) produced by neighboring electrons and nuclei. This additional interaction ability is due to a nuclear electric quadrupole moment (eQ), which, for sodium, is often quite strong, and can contribute significantly to the appearance and characteristics of the acquired NMR spectrum. There are three possible cases for quadrupole effects on the sodium spectrum: anisotropic molecular motion, rapid isotropic molecular motion, and slow isotropic molecular motion (Schmidt and Rosett 1995).

2.2.2.2 Anisotropic Molecular Motion: Quadrupole Splitting

The sodium nuclei can undergo three different energy level transitions: -3/2 to -1/2, -1/2 to +1/2, and +1/2 to +3/2. In the case of anisotropic molecular motion, these three transitions can appear as three distinct peaks on the NMR spectrum. The central peak (representing the -1/2 to +1/2 transition) contains 40% of the total intensity, while the two outer peaks each contain 30% of the total intensity (Figure 2.6). The distance between two neighboring peaks is known as quadrupole splitting (Δ) (Rooney and others 1987).

2.2.2.3 Rapid Isotropic Molecular Motion: Extreme Narrowing

In the case of liquids, which undergo rapid isotropic molecular motions, the electric field gradient is not more likely to point in one direction over another; therefore, no splitting is observed, and only one peak is obtained (Figure 2.7). Extreme narrowing holds true when the correlation time, τ_c, which describes the fluctuations in the electric field gradient at the nucleus, is very small compared to the inverse resonant frequency. In this case, T_1 and T_2 are equal (Lerner and Torchia 1986).

2.2.2.4 Slow Isotropic Molecular Motion: Nonextreme Narrowing

In the case where the correlation time cannot be neglected because of its small size compared to the inverse resonant frequency, nonextreme narrowing occurs. In this situation, the spectrum will appear to be one peak, but in reality, it is the superposition of two Lorentzian peaks (Figure 2.8). One of the signals comprises 60% of the overall peak, and is characterized by a broad linewidth. This signal is the rapidly relaxing component (T_{2f}^{SQ}), corresponding to the -3/2 to -1/2 and 1/2 to 3/2 transitions. The other signal makes up 40% of the overall peak and is characterized by a narrow linewidth. This component corresponds to the -1/2 to 1/2 transition, and is slowly relaxing (T_{2s}^{SQ}) (Delville and others 1978).

2.2.3 ^{23}Na NMR Experiments: Single Quantum

Information about the total sodium population can be obtained from the single quantum (SQ) pulse sequence. T_1^{SQ} allows for the characterization of sodium ion mobility – the longer the longitudinal relaxation time, the more mobile the sodium ions. The T_1^{SQ} relaxation curve exhibits a mono-exponential behavior, which indicates that if two pools of sodium are present in the sample, the exchange rate between the two pools is too fast to allow any discrimination by T_1 measurements.

In the case of the T_2 parameter, the extreme narrowing conditions do not hold, and a bi-exponential function is necessary to fit the T_2^{SQ} decaying components. The evolution curve of the signal intensity (I_{T2}) is described as:

$$I_{T2}(t) = k * [P_{2s}^{SQ} * \exp(-t/T_{2s}^{SQ}) + P_{2f}^{SQ} * \exp(-t/T_{2f}^{SQ})] \quad (2)$$

where k is a constant, T_{2s}^{SQ} and T_{2f}^{SQ} are the slow and fast components of T_2^{SQ}, and P_{2s}^{SQ} and P_{2f}^{SQ} are their relative populations ($P_{2s}^{SQ} \approx 0.4$; $P_{2f}^{SQ} \approx 0.6$) (Gobet and others 2010).

2.2.4 ^{23}Na NMR Experiments: Double Quantum Filtered

The double quantum filtered (DQF) pulse sequence is able to selectively measure the bound (or associated, restricted) sodium population in the sample by eliminating SQ coherences, leaving only DQ coherences in the signal. The phase-cycled pulse sequence, which selects DQ coherences, is:

$$(\pi/2)_\varphi - \tau/2 - (\pi)_{\varphi+90} - \tau/2 - (\pi/2)_\varphi - \delta - (\pi/2)_\varphi - Acq(t)_\varphi \quad (3)$$

where τ is the creation time and δ is the DQ evolution time. To eliminate the SQ coherences, a four-step phase cycle is used where ϕ = 0°, 90°, 180°, 270° and ϕ' = 2(0°, 180°), thus only corresponding to bound sodium in the sample. The resultant DQF peak can be deconvoluted into two Lorentzian lines, of equal areas, but different widths, in antiphase (Figure 2.9). The two DQ

lines are characterized by two different relaxation times: the 'fast' (T_{2f}^{DQ}, broad line) and 'slow' (T_{2s}^{DQ}, narrow line). The T_{2f}^{DQ} and T_{2s}^{DQ} components are determined by fitting a curve of the DQF signal intensity (I_{DQ}) as a function of τ according to the equation (Figure 2.10):

$$I_{DQ} = k * [\exp(-\tau/T_{2s}^{DQ}) - \exp(-\tau/T_{2f}^{DQ})] \quad (4)$$

The optimum duration of τ that maximizes the amplitude of the DQ signal can be calculated using the equation:

$$\tau^{opt} = \ln(R_{2f}/R_{2s})/(R_{2f} - R_{2s}) \quad (5)$$

where $R_{2s} = 1/ T_{2s}^{DQ}$ and $R_{2f} = T_{2f}^{DQ}$. The mathematical derivations of the DQF equations have been previously reported in the literature (Jaccard and others 1986; Whang and others 1994; Kemp-Harper and others 1997; Woessner 2001).

2.2.4.1 Absolute Quantification of Bound Sodium

When B_1 is homogeneous and δ is on the scale of microseconds, the phase cycle that selects DQ coherences (Equation 3) produces a detectable DQF free induction decay at resonance, which is described by Equation 6,

$$M(t,\tau) = M_0 \left(\frac{3}{20}\right) [\exp\left(-\frac{\tau^{opt}}{T_{2S}}\right) - \exp\left(-\frac{\tau^{opt}}{T_{2F}}\right) * [\exp\left(-\frac{t}{T_{2S}^*}\right) - \exp\left(-\frac{t}{T_{2F}^*}\right)] \quad (6)$$

where M_0 is the equilibrium longitudinal magnetization, and T^*_{2S} and T^*_{2F} are related to T_{2S} and T_{2F}, after the magnetic field inhomogeneity, due to B_0, is taken into account (Equation 7).

$$\frac{1}{T_{2i}^*} = \frac{1}{T_{2i}} + \gamma\Delta B_0 \qquad (i = S \text{ or } F) \quad (7)$$

$\gamma\Delta B_0$ is the inhomogeneity factor that accounts for the line broadening as a result of B_0, and can be calculated with Equation 7 by using the T_2^{SQ} relaxation time and determining T_2^* from Equation 8, where $W_{1/2}$ is the natural linewidth at half height of a SQ peak:

$$W_{1/2} = 1/\pi T_2^* \quad (8)$$

Equation 6 undergoes Fourier transform, and the amplitude of the resulting spectrum is described by Equation 9:

$$S(\omega,\tau) = M_0\left(\frac{3}{20}\right)\left[\exp\left(-\frac{\tau^{opt}}{T_{2S}}\right) - \exp\left(-\frac{\tau^{opt}}{T_{2F}}\right)\right]F(\omega) \quad (9)$$

F(ω), depicted in Equation 10, is the lineshape function,

$$F(\omega) = \frac{R^*_{2S}}{R^{*2}_{2S}+\omega^2} - \frac{R^*_{2F}}{R^{*2}_{2F}+\omega^2} \quad (10)$$

where R^*_{2S} and R^*_{2F} are the inverse of T^*_{2S} and T^*_{2F}, respectively. Because the area under the DQ peak is the integral of the lineshape function *F(ω)* (Equation 10) between the two zero derivative points, defined by ±ω' (Figure 2.11), Equation 6 can be re-written as Equation 11, to describe the area under the peak:

$$A^{DQ} = M_0\left(\frac{3}{20}\right)\left[\exp\left(-\frac{\tau^{opt}}{T_{2S}}\right) - \exp\left(-\frac{\tau^{opt}}{T_{2F}}\right)\right] * [tan^{-1}(\omega' T^*_{2S}) - tan^{-1}(\omega' T^*_{2F})]$$

(11)

where ω' is described in Equation 12:

$$\omega' = \left[\frac{\sqrt{R^*_{2S}}R^{*2}_{2F} - \sqrt{R^*_{2F}}R^{*2}_{2S}}{\sqrt{R^*_{2F}} - \sqrt{R^*_{2S}}}\right]^{1/2} \quad (12)$$

M_0 can be related to the concentration of bound sodium ions through the use of an external saline reference, such as $Na_7Dy(PPP)_2$, of magnitude M_{REF}, that has a frequency shifted away from the ^{23}Na resonance of the sample. Equation 13 can be used to describe the area under the SQ reference peak,

$$A^{SQ}_{REF} = M_{REF}\pi \quad (13)$$

and it can be combined with Equation 11 to calculate M_0, which is described by Equation 14,

$$M_0 = M_{REF}\left(\frac{10\pi}{3}\right)\frac{A^{DQ}}{A^{SQ}_{REF}}\frac{N^{SQ}}{N^{DQ}}\left[\exp\left(-\frac{\tau^{opt}}{T_{2S}}\right) - \exp\left(-\frac{\tau^{opt}}{T_{2F}}\right)\right]^{-1} * [tan^{-1}(\omega' T^*_{2S}) - tan^{-1}(\omega' T^*_{2F})]^{-1} \quad (14)$$

where N^{SQ} and N^{DQ} are the number of scans acquired in SQ and DQ experiments, respectively. Because the DQ and SQ spectra were both collected using 1024 scans, in this experiment, the equation for calculating the absolute concentration of bound sodium is shown in Equation 15 (Mouaddab and others 2007).

$$[Na^+]^{DQ}_{CALC} = [Na^+]^{SQ}\left(\frac{10\pi}{3}\right)\frac{A^{DQ}}{A^{SQ}_{REF}}\left[\exp\left(-\frac{\tau^{opt}}{T_{2S}}\right) - \exp\left(-\frac{\tau^{opt}}{T_{2F}}\right)\right]^{-1} * [tan^{-1}(\omega' T^*_{2S}) - tan^{-1}(\omega' T^*_{2F})]^{-1} \quad (15)$$

The use of Equation 15 to absolutely quantify the concentration of bound sodium in food has only been reported in 3 previous papers – one investigating sodium binding to gluten in bread (Guojonsdottir and others 2013), another looking at sodium binding in a model cheese system (Boisard and others 2014), and a third correlating sodium ion binding to proteins and salty taste perception in protein matrices (Mosca and others 2015). Even though the absolute quantification of bound and free sodium ions was not reported by Gobet and others 2009b), we wanted to attempt the calculation with the iota-carrageenan sample, to investigate if the equation could be applied to that system.

2.2.5 Iota-carrageenan

Iota-carrageenan is produced from the red seaweed *Eucheuma denticulatum*, and is a polysaccharide comprised of repeating galactose and 3,6-anydrogalactose units (3,6-AG) (Figure 2.12). Each disaccharide repeating unit has an average of 2 sulfate groups, but the exact degree of sulfation varies depending on the source and extraction process (Falshaw and others 2001). There are two different methods to produce carrageenan – one method produces refined carrageenan, while the other method produces semi-refined carrageenan. To make refined carrageenan, a base, like sodium hydroxide, is used to extract the carrageenan from the seaweed into solution. It is then precipitated out of solution using isopropanol, dried, and ground. For semi-refined carrageenan, the carrageenan is not extracted from the seaweed – the starting

material is soaked in KOH, in which soluble proteins, carbohydrates, and salts dissolve. However, the potassium prevents the carrageenan from going into solution. Then the carrageenan and other insoluble material (mainly cellulose) is dried and ground. In each of these processes, the alkali solution removes some sulfate groups and increases the formation of 3,6-AG. Therefore, the number of sulfate groups varies depending on how long and at what temperature the seaweed sits in the alkali solution (McHugh 2003).

The gelation mechanism for iota-carrageenan as the NaCl concentration increases has been investigated in previous studies (Gobet and others 2009). It was found that there are three [NaCl]-dependent stages of iota-carrageenan gelation (Figure 2.13). In the first stage, at low concentrations of added NaCl, carrageenan chains are in random-coil confirmation, and there is no bound sodium. In stage two, as the concentration of added NaCl increases, carrageenan strands adopt a double helix conformation, and the bound fraction of sodium increases. In the third stage, all of the sodium binding sites on the carrageenan are occupied.

The stages of gel formation in iota-carrageenan are supported by the sodium binding trends as the concentration of added NaCl increases. As seen in Figure 2.14, the ratio of bound to total sodium (A_{DQ}/A_{SQ}) increases during stage two, indicating the amount of bound sodium increases as the concentration of added NaCl increases. During stage three, the ratio of bound to total sodium decreases, which could indicate that the binding sites become saturated and additional sodium is no longer binding to the carrageenan. For the validation experiments, 0.40 M added NaCl was chosen because it is located in region 3, and it was thought that if all of the sodium was bound, there would be less opportunity for error.

2.3 Experimental

2.3.1 Sample Preparation

1% (w/w) iota-carrageenan with 0.40 M added NaCl samples were prepared by adding the NaCl (Certified ACS Crystalline, Fisher Scientific, Fair Lawn, NJ, USA) to deionized water, and stirring with a stir bar at room temperature (22 °C) until the NaCl dissolved. The iota-carrageenan (Ticaloid 100 Powder, TIC Gums, Belcamp, MD, USA) was then added to the NaCl-water solution, and it was heated and stirred until the mixture became translucent and hydrocolloid particles were no longer visible. The sample was pipetted into a 5 mm thin wall precision NMR tube (528-PP-7, Wilmad-LabGlass, Vineland, NJ, USA) that had been heated in boiling water for 10 minutes, in order to warm the tube to prevent the gel from setting immediately on contact. A 0.0571 M $Na_7Dy(PPP)_2$ (0.40 M Na^+) aqueous solution was prepared by combining 2.50 mL of 0.230 M $Na_5(PPP)$ (Fisher Scientific, Fair Lawn, NJ, USA) with 2.50 mL of 0.113 M $DyCl_3 \bullet 6H_2O$ (Strem Chemicals, Newburyport, MA, USA) in D_2O, and was used as an external reference to verify the sodium ion concentration of the carrageenan sample. $Dy(PPP)_2^{7-}$ was chosen as the anion for the reference because it induces an upfield shift of Na^+, so the reference sodium peak could be distinguished from the sample peak. The reference solution was pipetted into a 2 mm coaxial NMR tube (NE-5-CIC-V, New Era Enterprises, Inc., Vineland, NJ, USA), and was secured inside the 5 mm tube containing the carrageenan sample.

2.3.2 ^{23}Na NMR Parameters

^{23}Na SQ and DQF experiments were recorded at 158.660 MHz on a Varian Unity Inova 600 MHz (14.09 T) spectrometer equipped with a 5-mm Varian AutoTuneX ^{1}H/^{23}Na broadband probe. The $\pi/2$ pulse length was optimized for each sample, which ranged from 15.0 to 17.5 ms. The longitudinal relaxation time, T_1, was determined from the inversion-recovery (IR) pulse sequence, using 15 inter-pulse delays from 0.125 to 2048 ms. A Carr-Purcell-Meiboom-Gill

(CPMG) pulse sequence employing 31 echo times from 0.375 to 1536 ms, and an echo time of 200 μs was used to determine T_2 for the samples. All experiments were performed with a delay between scans (repetition time) of 200 ms. In order to determine τ^{opt}, DQF spectra were acquired with δ = 10 μs for 31 τ values, ranging from 100 μs to 40 ms. All acquisitions for SQ and DQF experiments were recorded with an identical number of scans (1024), recycle delays (200 ms), and receiver gains. All experiments were conducted at room temperature (between 21.8 and 22.2 °C).

2.3.3 Data Processing

SQ and DQF spectra were integrated using Microsoft Excel 2010 (Microsoft Corporation, Redmond, WA, USA), using the trapezoidal rule as an approximation, which is shown in Equation 16.

$$\int_a^b f(x)dx \approx (b-a)\left[\frac{f(a)+f(b)}{2}\right] \quad (16)$$

The method calculates the area of a trapezoid between individual time points (a and b), and then sums the areas of the individual trapezoids to determine the approximate area under the curve. The difference between a and b for the samples was 1.9 ms, and between 700 and 3600 time points were used.

Previous studies used PeakFit software (Version 4.12, SeaSolve Software Inc., San Jose, CA, USA) to determine the area under the peaks. In PeakFit, the DQF peak can be deconvoluted into a narrower positive peak above the baseline, and a broader negative peak below the baseline (Figure 2.9). Theoretically, these two peaks are equal in area, and are also equal to the area of the DQF peak (Mouaddab and others 2007). However, when fitting the peaks using the PeakFit software, the area of the positive peak did not always equal the area of the negative peak (Table 2.1). When the positive peak areas were plotted versus tau (Figure 2.15), a higher variation was

observed in the fitting (R^2 = 0.966), compared to when the trapezoidal rule was applied to approximate the area of the DQF peaks (R^2 = 0.9847) using Microsoft Excel (Figure 2.16). Therefore, the trapezoidal approximation using Microsoft Excel was used to determine the area of the SQ and DQF peaks.

2.4. Results and Discussion

2.4.1 Verification of Sodium Ion Concentration

The concentration of sodium ions in the carrageenan sample was verified using Equation 17,

$$[Na^+]^{SQ} = \frac{A^{SQ}}{A^{SQ}_{REF}} * \frac{V_{Inner}}{V_{Outer}} * [Na^+]^{SQ}_{REF} \quad (17)$$

where A^{SQ} and A^{SQ}_{REF} are the peak areas of the carrageenan and external reference SQ signals, respectively, V_{Inner}/V_{Outer} is the volume ratio of the inner coaxial tube to the outer tube, and $[Na^+]^{SQ}_{REF}$ is the sodium ion concentration in the external reference. The $[Na^+]^{SQ}$ value determined using Equation 17 was 0.374 M, which is in close agreement with the expected value of 0.413 M (9% difference). The calculated sodium ion concentration values for a resin system in the original methods paper deviated between 1% and 6% from the expected values (Mouaddab and others 2007). The increased difference in this carrageenan experiment could be due to product loss when making the samples. Even with 9% error, the calculated value is still in close agreement with the expected value, and thus indicates that all ions, even the ones exhibiting restricted mobility, are detected by the SQ NMR method (Mouaddab and others 2007).

2.4.2 Comparison of T_1 values

The T_1 value for this current carrageenan sample was found to be 47.71 ms, which is in very close agreement with the literature value of about 48 ms for the 0.40 M NaCl carrageenan sample (Gobet and others 2009b).

2.4.3 Comparison of τ^{opt} values

The signal intensities of DQF T_2 peaks were measured at tau values ranging from 100 μs to 40 ms, and are plotted in Figure 2.16. The curve was fitted using Equation 4, and τ^{opt} was determined to be 18.3 ms, using Mnova NMR (Version 8.1, Mestrelab Research, Santiago de Compostela, Spain). However, the τ^{opt} in the literature was reported as about 12 ms for the 0.40M added NaCl carrageenan sample (Gobet and others 2009b). The differences in the optimum tau value could be due to the differences in carrageenan samples between this study and the literature experiment. In the literature, a specific type of carrageenan was not specified (only that it was acquired from Rhodia Food in Aubervilliers, France). For this study, a fully refined sample of iota-carrageenan, specifically Ticaloid 100 Powder, was acquired from TIC Gums in Belcamp, MD. It is not known whether the sample from Rhodia Food was fully refined or semi-refined, which would have an effect on the number of available sulfate binding sites. In addition, the processing conditions would have an effect on the number of sulfate groups, as well – iota-carrageenan contains an average of 2 sulfate groups per disaccharide, but the exact degree of sulfation varies. In addition, the pK_a of the iota-carrageenan samples could have varied as well, which would affect the number of negatively charged sulfate groups available for the sodium to bind. The degree of binding could lead to a difference in the ordering of the environment in which the sodium ions are contained, and thus vary optimum tau values.

It was later seen with the emulsion samples in Chapter 3 that Equation 4 does not apply in all systems for the fitting of the curve to determine τ^{opt}. As seen with the 250 mg added Na

reduced-fat emulsion sample, the τ^{opt} from the fitted curve is about 8 ms, whereas the actual τ^{opt}, determined by inspection, appears to be around 10 ms (Figure 2.17). Mnova NMR, Microsoft Excel, and MATLAB (Version R2015a, MathWorks, Natick, MA, USA) were all utilized to attempt to more accurately fit the curve, all with unsuccessful results (Table 2.2). In study investigating the model resin system, the reported DQ T_{2S} and T_{2F} values were 12.7 ms and 2.3 ms, respectively (Mouaddab and others 2007). However, as seen in Table 2.2, both T_{2S} and T_{2F} were found to be about 8 ms. The fact that T_{2S} and T_{2F} were found to be essentially equal for our carrageenan system could be one reason for the equation not fitting the data. It is possible that this lack of good fit is due to the complexity of the sample - different components relax at different rates, and there are not enough terms in the equation to account for each separate relaxation. However, previous studies that investigated cheeses and bread were able to very accurately fit the curve to the data using Equation 4, and calculate an absolute concentration of bound sodium using Equation 15, so there may be other factors present that lead to the inaccurate fitting.

2.4.4 Comparison of Relative Quantification of Bound Sodium (A_{DQ}/A_{SQ})

The area of the DQF T_2 peak, representing the population of bound sodium ions in the sample, can be compared to the area of the total sodium peak in order to gain insight about the relative quantification of bound sodium in the sample. The comparison of peaks does not allow for an absolute quantification, as shown in a model resin system - when all of the binding sites were occupied by Na^+, so that 100% of the sodium in the system was bound, the DQF peak was only 2.2% of the total sodium concentration, instead of 100% (Mouaddab and others 2007). It was proposed that this difference is due to a high magnetic field inhomogeneity, likely due to an internal magnetic field susceptibility effect (the presence of small air bubbles) (Mouaddab and

others 2007). Even though absolute values cannot be determined by the peak ratios, a relative percentage of bound sodium can be determined for a system.

For the carrageenan sample in the literature, at 0.4 M added NaCl, the ratio of the double quantum area to the single quantum area is about 11% (Figure 2.14) (Gobet and others 2009b). In this study, the comparison of peak areas indicated that only 0.14% of the sodium was bound in the sample. However, the ratio is a relative ratio, and can only be compared to samples within the same system, measured using the same instrument. Neither percentage is an absolute percentage of bound sodium. It would be expected that if carrageenan samples were run at all added sodium concentrations tested in the literature, that a similar trend in sodium binding would be observed (the ratio would be zero, then increase, then decrease as sodium concentration increases). However, because only one concentration of added sodium was tested, this hypothesis cannot be verified. The discrepancy in relative percent bound sodium in the carrageenan samples could also be due to the differences in carrageenan sample tested. Differences in source, degree of sulfation, or degree of refinement could affect the exact number of sulfate groups available for binding, affecting the mobility of those sodium ions in the carrageenan environment.

2.4.5 Absolute Concentration of Bound Sodium

Some previous studies have shown that the absolute concentration of bound sodium in the sample can be calculated using Equation 15 (Mouaddab and others 2007, Guojonsdottir and others 2013, Boisard and others 2014). However, when the equation was applied to the carrageenan data collected, the calculation indicated that 6920% of the sodium is bound in the samples (Table 2.3). Because the maximum feasible percentage of bound sodium in the sample is 100%, the equation does not accurately calculate the absolute concentration of bound sodium in the carrageenan sample. Although the carrageenan study in the literature (Gobet and others

2009b) was published after the first paper in the literature that describes the equation for the absolute quantification of bound sodium (Mouaddab and others 2007), the equation was not mentioned in the carrageenan paper (Gobet and others 2009b). The equation was also absent from additional papers that utilized the DQF pulse sequence to investigate bound sodium in different cheeses and model cheeses (Gobet and others 2009a, Gobet and others 2010, Boisard and others 2013). The omission of this equation in multiple studies could indicate that it is not applicable to all systems.

2.5 Conclusions

As a result of this study, the SQ and DQF NMR methods have been implemented and verified at the University of Illinois at Urbana-Champaign, by comparing results of an iota-carrageenan sample (1% (w/w)) with 0.40 M added NaCl to literature values. It was shown that the NMR detected all of the sodium in the sample, and the T_1 values very closely matched literature values. The optimum tau value and the relative percentage of bound sodium in the sample differed from reported values, which could be due to differences in the iota-carrageenan samples used, specifically degree of sulfation of the specific iota-carrageenan samples. However, despite these differences, and despite not being able to accurately calculate the absolute percentage of bound sodium in the sample, the ratio of bound to total sodium peak areas is still a useful measure to investigate the mobility of bound sodium in samples, and it can be used for relative quantification of bound sodium in the system. The application of this method to a model emulsion system for relative quantification will be discussed in Chapter 3.

2.6 References

Boisard L, Andriot I, Arnould C, Achilleos C, Salles C, Guichard E. 2013. Structure and composition of model cheeses influence sodium NMR mobility, kinetics of sodium release and sodium partition coefficients. Food Chemistry 136:1070-1077.

Boisard L, Andriot I, Martin C, Septier C, Boissard V, Salles C, Guichard E. 2014. The salt and lipid composition of model cheeses modifies in-mouth flavour release and perception related to the free sodium ion content. Food Chemistry 145:437-444.

Delville A, Detellier C, Laszlo P. 1978. Determination of the correlation time for a slowly reorienting spin-3/2 nucleus: binding of Na^+ with the 5'-GMP supramolecular assembly. Journal of Magnetic Resonance 34:301-315.

Falshaw R, Bixler HJ, Johndro K. 2001. Structure and performance of commercial kappa-2 carrageenan extracts: I. Structure analysis. Food Hydrocolloids 15:441-452.

Gobet M, Foucat L, Moreau C. 2009a. Investigation of sodium ions in cheeses by ^{23}Na NMR spectroscopy. In: Guojonsdottir M, Belton P, Webb G, eds. Magnetic Resonance in Food Science: Challenges in a Changing World. Cambridge, England:Royal Society of Chemistry p 57-64.

Gobet M, Mouaddab M, Cayot N, Bonny J-M, Guichard E, Le Quere J-L, Moreau C, Foucat L. 2009b. The effect of salt content on the structure of iota-carrageenan systems: ^{23}Na DQF NMR and rheological studies. Magnetic Resonance in Chemistry 47:307-312.

Gobet M, Rondeau-Mouro C, Buchin S, Le Quere J-L, Guichard E, Foucat L, Moreau C. 2010. Distribution and mobility of phosphates and sodium ions in cheese by solid-state ^{31}P and double-quantum filtered ^{23}Na NMR spectroscopy. Magnetic Resonance in Chemistry 48:297-303.

Guojonsdottir M, Traore A, Renou JP. 2013. The effect of crystal size and encapsulation of salt on sodium distribution and mobility in bread as studied with ^{23}Na Double Quantum Filtering NMR. In: van Duynhoven J, Belton PS, Webb GA, van As H, eds. Magnetic Resonance in Food Science: Food for Thought. Cambridge, England: Royal Society of Chemistry p 35-43.

Jaccard G, Wimperis S, Bodenhausen G. 1986. Multiple-quantum NMR spectroscopy of S=3/2 spins in isotropic phase: A new probe for multiexponential relaxation. J. Chem. Phys. 85:6282-6293.

Ionin BI and Ershov BA. 1970. The fundamentals of NMR spectroscopy. In: Ionin BI, Ed. NMR Spectroscopy in Organic Chemistry. Heidelberg, Germany: Springer p 1-59.

Kemp-Harper R, Brown SP, Hughes CE, Styles P, Wimperis S. 1997. Na-23 NMR methods for selective observation of sodium ions in ordered environments. Progress in Nuclear Magnetic Resonance Spectroscopy 30:157-181.

Lerner L and Torchia D. 1986. An analysis of non-Lorentzian ^{23}Na line shapes in two model systems. Journal of the American Chemical Society 108:4264-4268.

McHugh DJ. 2003. A guide to the seaweed industry. Rome, Italy: Food and Agriculture Organization of the United Nations. Fisheries Technical Paper #441. 105 p.

Mouaddab M, Foucat L, Donnat JP, Renou JP, Bonny JM. 2007. Absolute quantification of Na^+ bound fraction by double-quantum filtered ^{23}Na NMR spectroscopy. Journal of Magnetic Resonance 189:151-155.

MRI Basics. 2015. Cardiff, UK: Cardiff University, Experimental MRI Centre. Available from: www.cardiff.ac.uk. Accessed Apr 28, 2015.

Nitz WR, Balzer T, Grosu DS, Allkemper T. 2010. Principles of Magnetic Resonance. In: Reimer P, Parizel PM, Meaney JFM, Stichnoth FA, eds. Clinical MR Imaging. Heidelberg, Germany: Springer p 1-105.

Origin, Current Status, Future Developments of Neutron Backscattering. 2009. Available from: ah-backscattering.pagesperso-orange.fr. Accessed Apr 28, 2015.

Qu X, Guo D, Cao X, Cai S, Chen Z. 2011. Reconstruction of self-sparse 2D NMR spectra from undersampled data in the indirect dimension. Sensors 11(9):8888-8909.

Rooney WD, Barbara TM, Springer CS. 1988. Two-Dimensional Double-Quantum NMR spectroscopy of isolated spin 3/2 systems: ^{23}Na examples. Journal of the American Chemical Society 110:674-681.

Schmidt SJ and Rosett TR. 1995. Use of ^{23}Na NMR to study sodium-macromolecule interactions. In: Gaonkar AG, ed. Effects on Food Quality. New York, NY: Marcel Dekker, Inc p 13-42.

Whang J, Katz J, Boxt LM, Reagan K, Sorce DJ, Sciaca RR, Cannon PJ. 1994. Multiple-Quantum-Filtered NMR Determination of equilibrium magnetization for ^{23}Na quantitation in model phantoms. Journal of Magnetic Resonance, Series B 103:175-179.

Woessner DE. 2001. NMR Relaxation of Spin-3/2 Nuclei: Effects of structure, order, and dynamics in aqueous heterogeneous systems. Concepts in Magnetic Resonance 13(5):294-325).

2.7 Figures and Tables

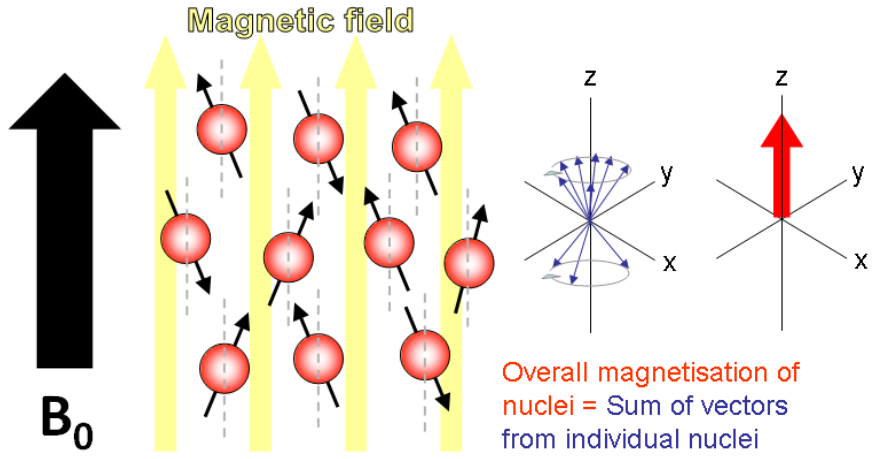

Figure 2.1. An example of the orientation of nuclei in the presence of an external magnetic field (Adapted from MRI Basics 2015).

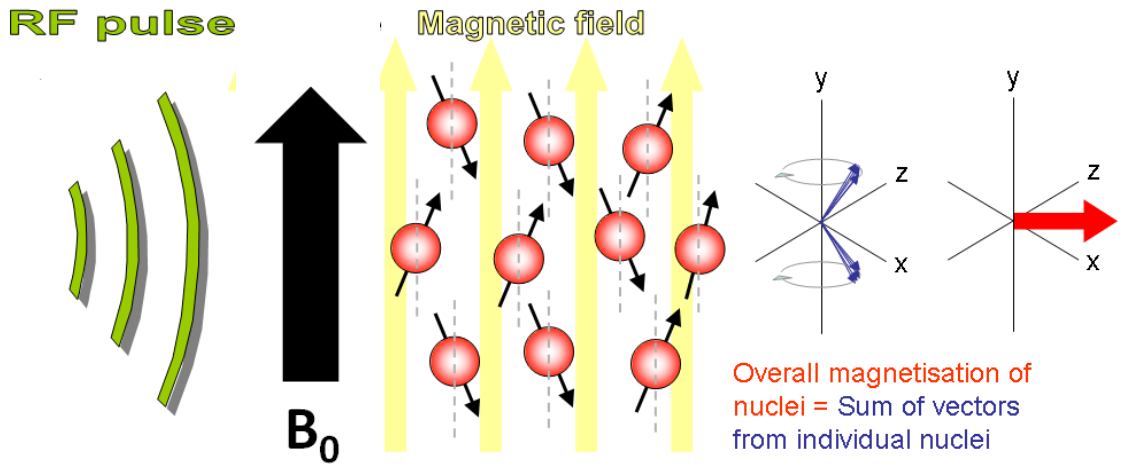

Figure 2.2. The magnetization of nuclei when a B1 pulse is applied (Adapted from MRI Basics 2015).

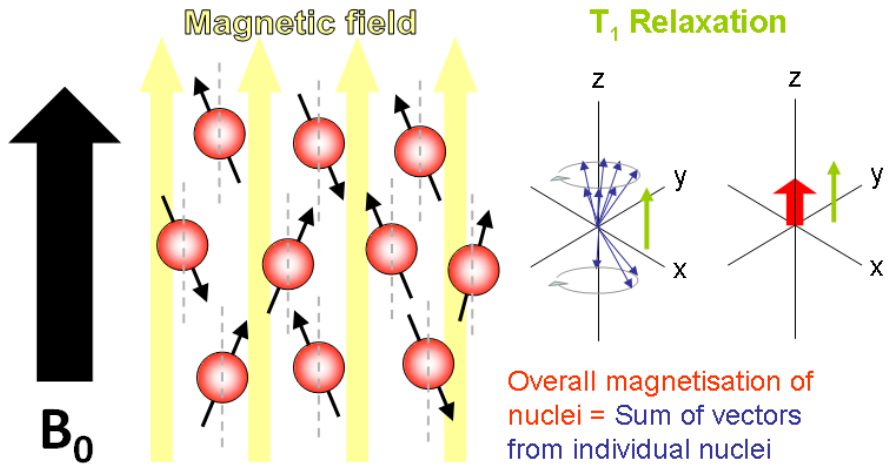

Figure 2.3. T1 (Longitudinal) Relaxation (Adapted from MRI Basics 2015).

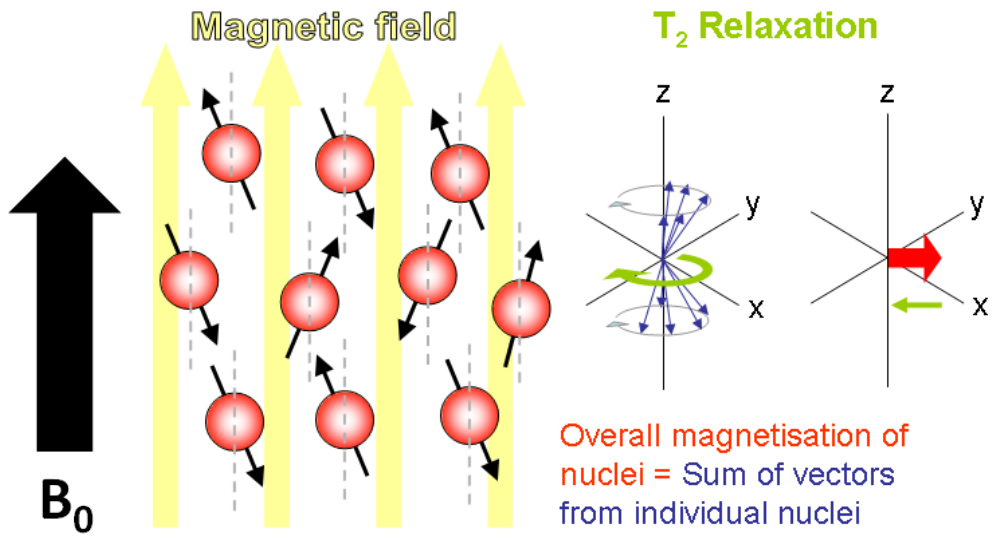

Figure 2.4. T2 (Transverse) Relaxation (Adapted from MRI Basics 2015).

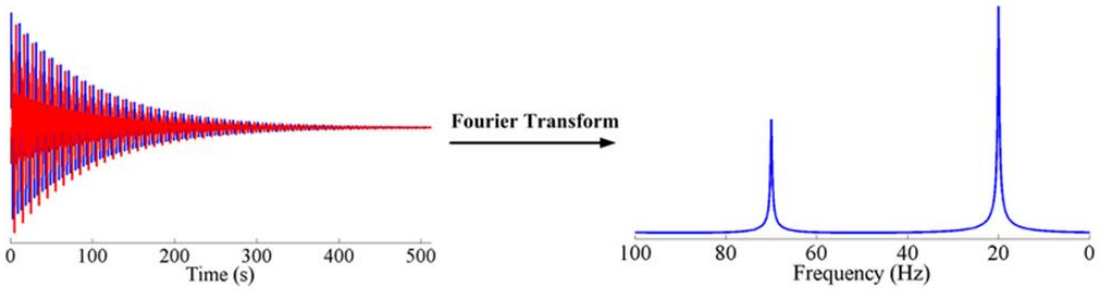

Figure 2.5. NMR time domain to frequency domain via Fourier Transform (FT) (Adapted from Qu and others 2011).

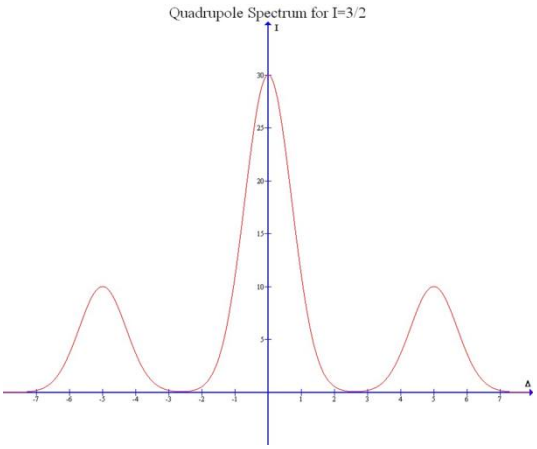

Figure 2.6. NMR spectra for I=3/2 anisotropic molecular motion (Excerpted from Origin, Current Status, Future Developments of Neutron Backscattering 2009).

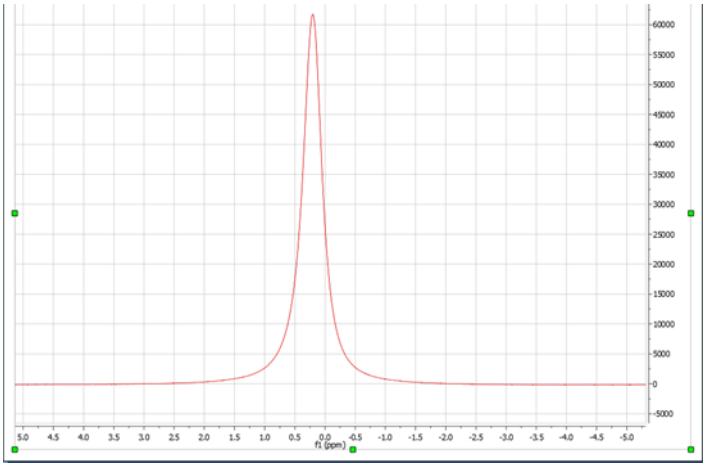

Figure 2.7. NMR spectra depicting rapid isotropic molecular motion: Extreme narrowing.

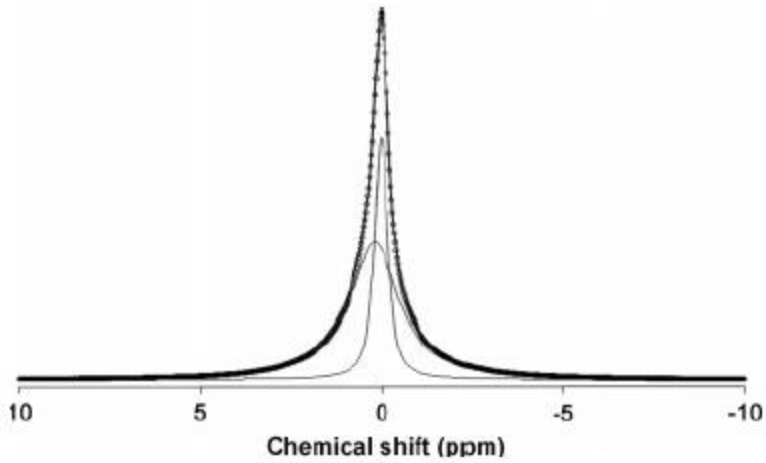

Figure 2.8. NMR spectra depicting slow isotropic molecular motion: Nonextreme narrowing condition. The total peak (darker line) is deconvoluted into two peaks. The taller, narrower peak accounts for 40% of the signal, while the shorter, broader peak accounts for 60% of the signal (Excerpted from Gobet and others 2010).

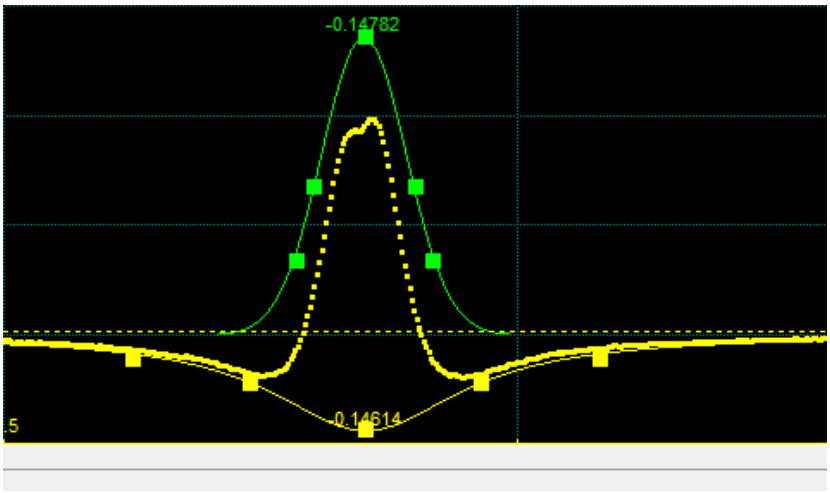

Figure 2.9. NMR spectrum depicting two lines in antiphase of equal areas, but different widths.

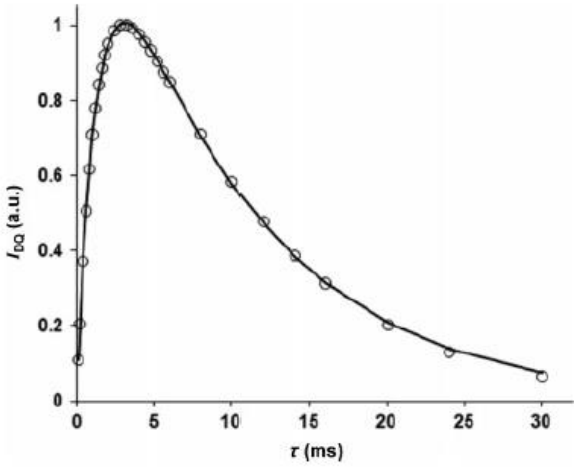

Figure 2.10. A representative curve of intensity versus time, used to determine the optimum tau value (Excerpted from Gobet and others 2010).

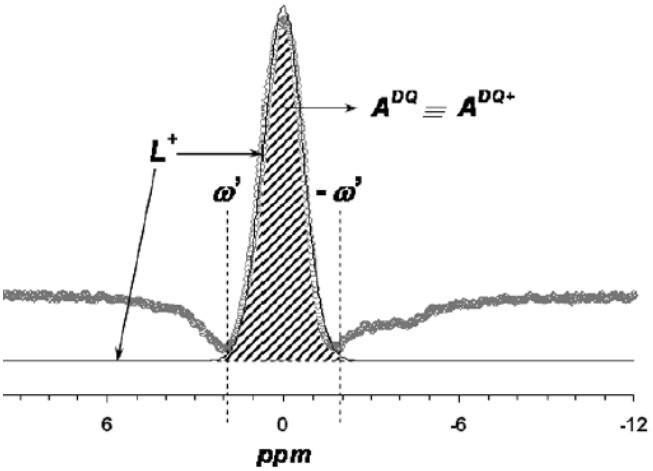

Figure 2.11. Experimental DQ spectrum of a resin sample. The lineshape form is given by Eq. (10) and the zero derivative points, ±ω', are defined in Eq. (12). The dashed area A^{DQ} is expressed by Eq. (11) (Excerpted from Mouaddab and others 2007).

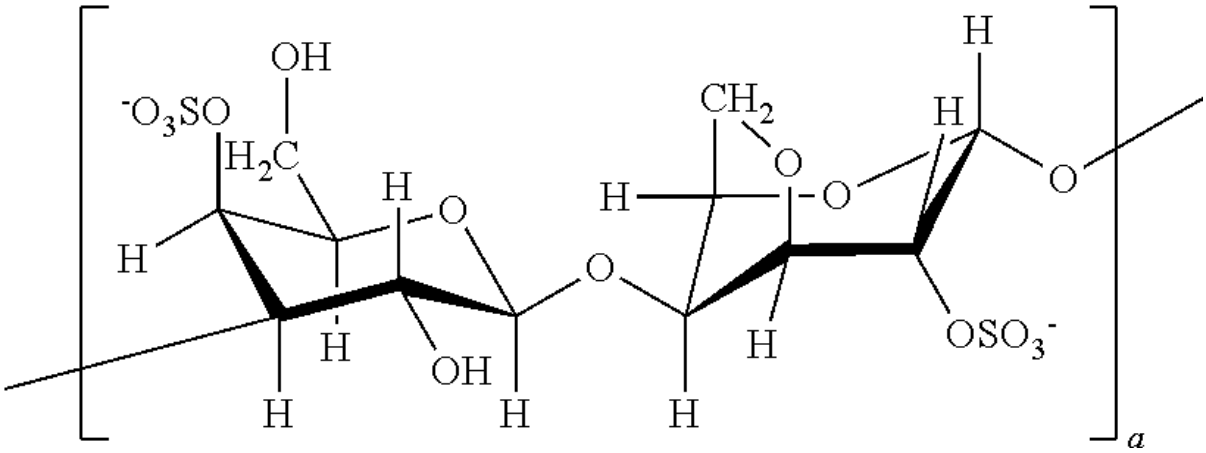

Figure 2.12. Structure of iota-carrageenan.

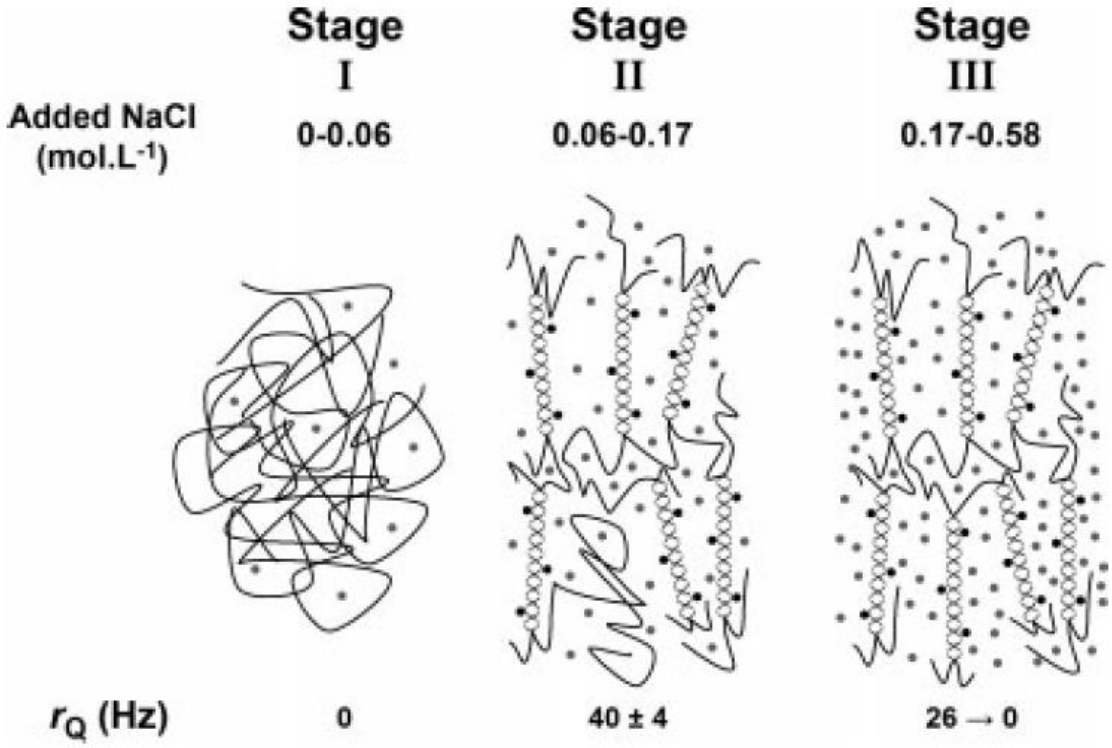

Figure 2.13. Schematic representation of the three [NaCl]-dependent stages of iota-carrageenan gelation. The free and bound sodium ions are symbolized by gray and black circles, respectively. The three delineated stages (I, II, III) match the three regions identified in Figure 2.14 (Excerpted from Gobet and others 2009b).

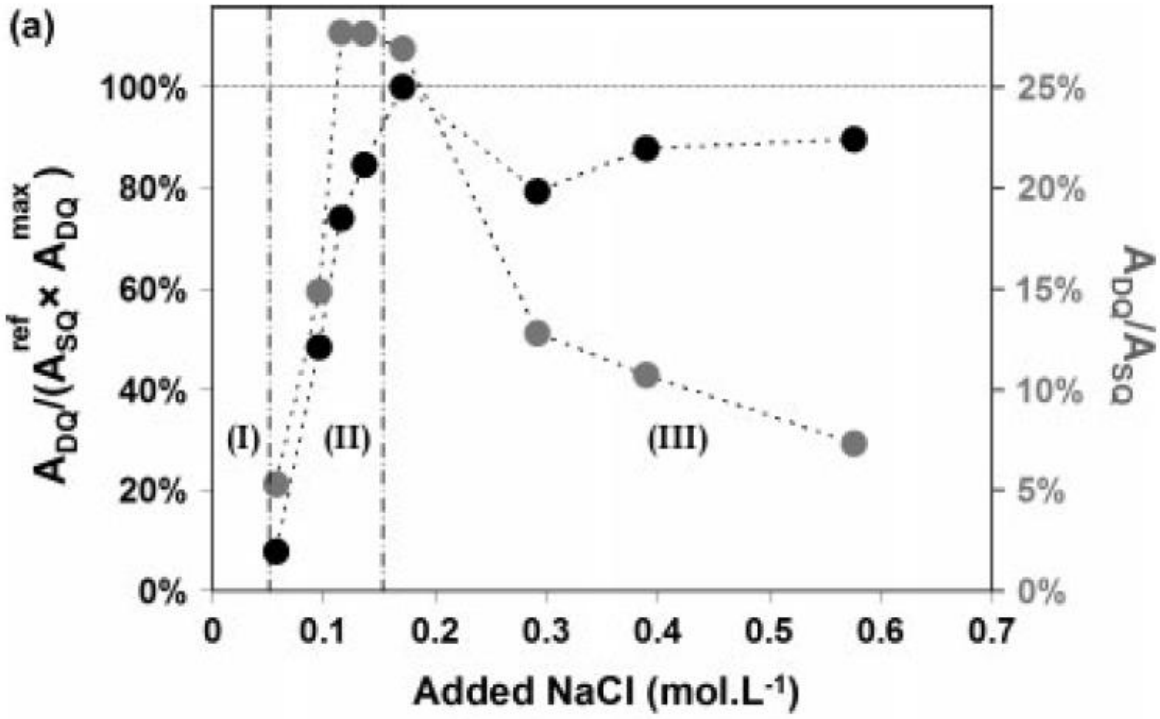

Figure 2.14. Evolution as functions of added NaCl content of $(A_{DQ})/(A_{SQ}^{ref} * A_{DQ}^{max})$ (black circles) and A_{DQ}/A_{SQ} (gray circles). Consecutive points are connected by straight lines. The three delineated regions (I, II, III) match the three stages proposed in Figure 2.13 (Excerpted from Gobet and others 2009b).

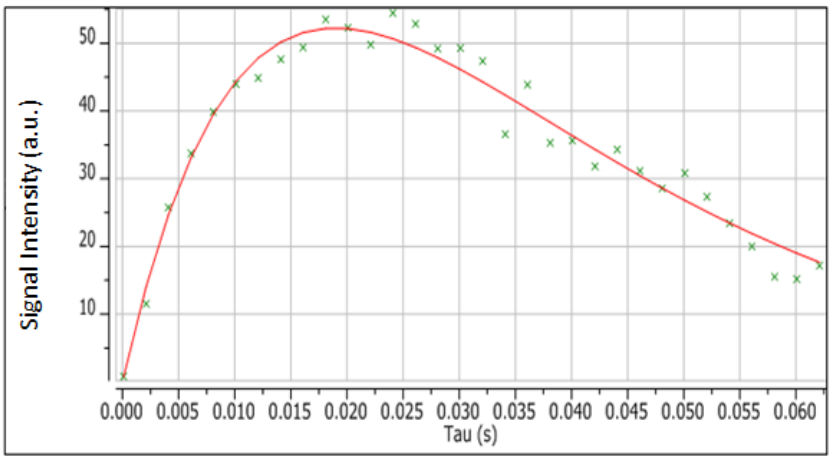

Figure 2.15. DQF peak area versus tau curve for a carrageenan sample, for which the areas were measured using PeakFit by deconvoluting the DQF peak into a positive and a negative peak to estimate the area of the DQF peak; the areas of the positive peak are plotted; a.u. refers to 'arbitrary unit'. The fitting was conducted using MNOVA software

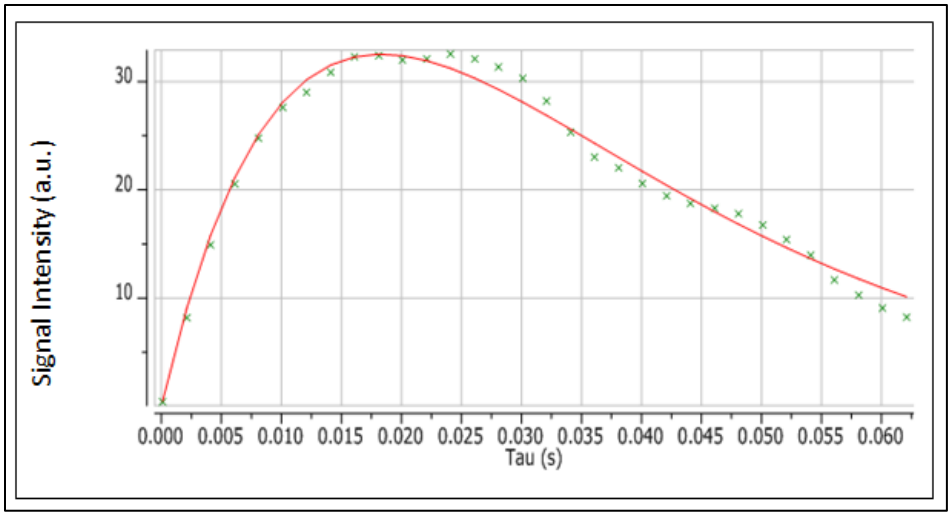

Figure 2.16**.** DQF peak area versus tau curve for a carrageenan sample, for which the areas were measured using Microsoft Excel by using the trapezoid rule. a.u. refers to 'arbitrary unit'. The fitting was conducted using MNOVA software.

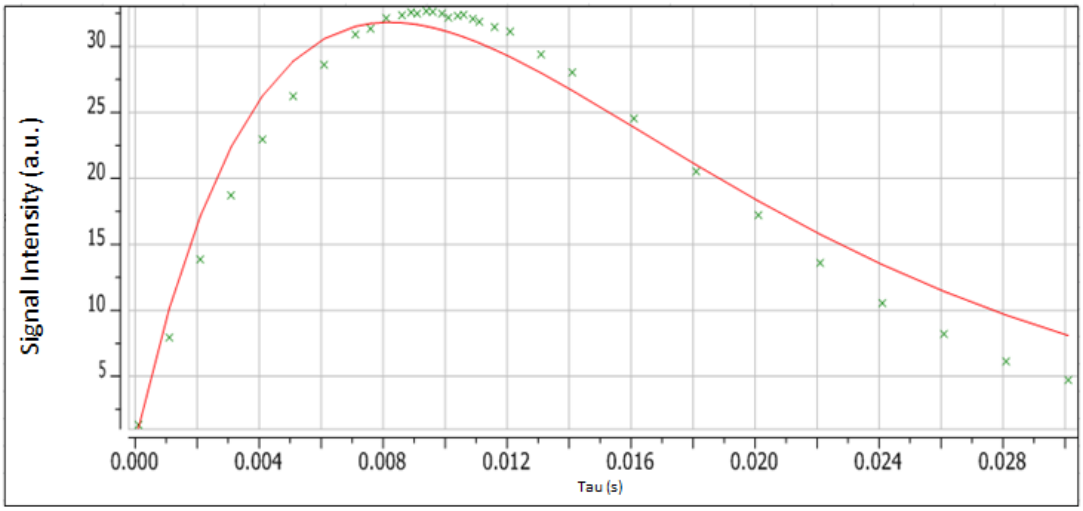

Figure 2.17. DQF peak areas versus tau (s) curve for 250 mg Na/serving, reduced-fat emulsion sample, for which the areas were measured using Microsoft Excel by using the trapezoid rule. a.u. refers to 'arbitrary units'. The fitting was conducted using MNOVA software.

Table 2.1. Areas of positive and negative peaks of carrageenan sample using PeakFit software and two lines in antiphase to fit the DQF T2 peaks, for 32 tau values ranging from 0.100 ms to 62.1 ms.

Tau (ms)	Positive Peak Area	Negative Peak Area
0.100	0.8008592	-0.616321
2.10	11.510682	-9.583044
4.10	25.763098	-24.22329
6.10	33.717399	-30.37097
8.10	39.87825	-37.2316
10.1	44.008383	-41.50988
12.1	44.921899	-40.68264
14.1	47.659359	-43.58574
16.1	49.396228	-45.22871
18.1	53.51661	-51.07992
20.1	52.245285	-49.56639
22.1	49.81894	-47.56825
24.1	54.450389	-51.4092
26.1	52.826042	-48.06972
28.1	49.187819	-44.52526
30.1	49.255193	-46.55249
32.1	47.335363	-43.87245
34.1	36.570156	-31.37067
36.1	43.90047	-42.68158
38.1	35.297453	-34.38635
40.1	35.615402	-32.3203
42.1	31.837085	-30.406
44.1	34.327926	-33.20883
46.1	31.127581	-29.68655
48.1	28.543791	-26.19123
50.1	30.796357	-27.43642
52.1	27.372583	-25.74912
54.1	23.40734	-22.67687
56.1	19.986334	-20.43224
58.1	15.498459	-15.37163
60.1	15.161554	-17.07407
62.1	17.190717	-15.91855

Table 2.2. Comparison of T_{2S}, T_{2F} and optimum tau values, for a 250 mg added sodium reduced-fat emulsion sample, calculated with three different fitting programs.

	MNOVA	**Excel**	**MATLAB**
T_{2S} (ms)	**8.38**	**8.42**	**8.40**
T_{2F} (ms)	**8.03**	**7.86**	**8.00**
τ^{opt} (ms)	**8.20**	**8.14**	**8.20**

Table 2.3. Relaxation times, inhomogeneity factor ($\gamma\Delta B_0$), optimal DQ creation time (τ^{opt}), and zero derivative point (ω') of the lineshape function $F(\omega)$ for Na^+ in carrageenan sample.

SQ Experiments	**DQ Experiments**	**SQ-DQ Combination**
T_2 = 42.8 ms	T_{2S} = 18.9 ms	T^*_{2S} = 16.7 ms
T_2^* = 33.2 ms	T_{2F} = 17.8 ms	T^*_{2F} = 15.9 ms
(↓Eq. (7))	(↓Eq. (5))	(↓Eq. (12))
$\gamma\Delta B_0 = 6.76\ s^{-1}$	τ^{opt} = 18.3 ms	$\omega' = 106$ rad s^{-1}

Chapter 3: Characterization of Sodium Binding and Viscosity in Full-Fat and Reduced-Fat Model Emulsion Systems

3.1 Abstract

Reduction of sodium in foods is a top priority in today's food industry. However, sodium reduction, due to its vital importance as a tastant, as well as its contribution to many other food properties, is no simple task. This study investigated the ionic binding of sodium ions to xanthan gum, a popular functional hydrocolloid used in many processed foods, and the effect of sodium ions on viscosity in full-fat and reduced-fat model emulsion systems with increasing concentrations of added sodium, from 0 to 480 mg added sodium per 30 gram serving. ^{23}Na NMR spectroscopy was utilized to determine sodium ion mobility, indicated by longitudinal (T_1) and transverse (T_2) relaxation times, and sodium binding, expressed by the ratio of bound to total sodium peak areas as the sodium concentration in the matrix increased. It was found that viscosity increased, then decreased with increasing sodium concentration, and the concentration at which it began to decrease was higher for the reduced-fat emulsion compared to the full-fat emulsion. The sodium mobility and sodium binding did not seem to be affected by pH. The characterization of sodium binding and viscosity in full-fat and reduced-fat model emulsion systems provides a foundation upon which further effects of sodium binding and functionality in food matrices can be investigated.

3.2 Introduction

Excessive intake of sodium is a major problem facing the United States and the world today. Overconsumption of sodium has been shown to cause an increased risk of high blood pressure, stroke, poor bone health, kidney disease, and stomach cancer (Kim and others 2012). The 2010 Dietary Guidelines for Americans suggests reducing sodium intake to less than 2,300

mg per day, with an even stricter recommendation of less than 1,500 mg per day for persons who are 51 and older, or those of any age who are African American or have hypertension, diabetes, or chronic kidney disease (USDA 2010). Despite these guidelines, Americans at or above the age of 2 consume on average over 3,400 mg of sodium per day (USDA 2005-2006). Of that sodium, only a small portion is added at the table – the majority of sodium is consumed from processed foods (USDA 2005-2006). However, the direct reduction of sodium from food products without replacement or other alterations would have a significant impact on many facets of the food system, including taste, microbial stability, flavor development, and texture formation, making sodium reduction a very complex and challenging problem (Kim and others 2012).

It has been shown that in specific processed food categories, including salad dressings, sodium contents are higher in lower-fat versions than their full-fat counterparts (Cox and Lee 2010). As sodium is being removed from food products, it is important to understand how the sodium interacts with different food components and affects food properties, such as texture.

^{23}Na Nuclear Magnetic Resonance (NMR) is a non-destructive, non-invasive method to determine the behavior of sodium ions in a system. There are a number of pulse sequences that can elucidate different information about the sodium ions in the system. The single quantum (SQ) pulse sequence can be utilized to determine the total amount of sodium in a sample, and the longitudinal (T_1) and transverse (T_2) can be used as a measure of total sodium ion mobility. However, in a food system, not all sodium ions exist in the same environment – some remain free (or unassociated), while others can bind, (or associate) with negatively charged amine and carboxyl groups in food macromolecules, such as in proteins and carbohydrates. When the sodium ions interact with these negatively charged groups, they exhibit restricted mobility, which can be measured using the double quantum-filtered (DQF) pulse sequence.

A recent study a study investigating protein matrices with varying types of protein (gelatin, milk protein, and soy protein), concentration of protein (2.5% and 9% w/w), and pH (6.8, 6.2, and 5.5) suggested that rheological properties, such as viscosity, have a larger effect on salty perception than sodium ionic binding and mobility (Mosca and others 2015). Therefore, the purpose of this study was to characterize and investigate sodium binding, sodium mobility, and viscosity in full-fat and reduced-fat model emulsion systems.

3.3 Materials and Methods

3.3.1 ^{23}Na NMR Experiments

3.3.1.1 Emulsion Preparation

The emulsions consisted of de-ionized water, soy lecithin (Solec WD, The Solae Company, St. Louis, MO, USA), Crisco Pure Vegetable Oil (The J.M. Smucker Company, Orrville, OH, USA), sodium chloride (No iodide added, Morton Salt, Inc., Chicago, IL, USA), and xanthan gum (NovaXan D; Archer Daniels Midland, Decatur, IL, USA). The formulations for the full-fat and reduced-fat emulsions at each sodium level are given in Tables 3.1 and 3.2. The exact and rounded sodium concentrations per 30 gram serving size are given in Tables 3.3 and 3.4; the rounded values will be used for ease of discussion throughout this paper.

Reduced-fat is defined as 25% less fat than an appropriate reference food (FDA 2013). Fourteen full-fat (40% fat) and fourteen reduced-fat (28% fat) emulsions were made at sodium concentrations ranging from 0 to 480 mg added sodium per 30 gram serving. The serving size selected represents the average serving size for commercial ranch dressings, and the sodium levels of commercial dressings also fall within the concentration range tested (see Table 3.5). Full-fat samples were made at added sodium concentrations of 0, 7, 65, 100, 130, 170, 200, 230, 265, 300, 350, 395, and 460 mg added sodium/serving. Reduced-fat samples were made at added

sodium concentrations of 0, 7, 35, 70, 140, 210, 220, 235, 250, 260, 280, 345, 410, and 480 mg added sodium/serving. In both the full-fat and reduced-fat emulsions, there was an endogenous sodium concentration of 6.29 mg sodium per serving from the xanthan gum, according to the nutritional information provided by ADM (see Appendix F).

Emulsions were made using a Vitamix TurboBlend Two Speed blender (Vita-Mix Corporation, Cleveland, Ohio, USA). First, the water and oil were blended on high speed (28,900 rpm) for 10 seconds. Then, approximately half of the oil was added to the carafe and blended at low speed (25,300 rpm). After 15 seconds, the remaining oil was slowly poured in the top opening of the carafe, with all of the oil being added after 30 seconds. The mixture was blended for an additional 30 seconds, for a total of 1 minute. Finally, the NaCl and xanthan gum were added to the mixture, and the emulsion was blended on high for 1 minute, and refrigerated at 2 °C.

The emulsions were made 12 to 28 hours before NMR and viscosity data were collected. One hour before the NMR experiments were run, samples were pipetted into 5mm NMR tubes and were allowed to equilibrate to room temperature (22 °C). For viscosity measurements, the samples were equilibrated to 25 °C before measurements were conducted.

3.3.1.2 ^{23}Na NMR Parameters and Data Processing

^{23}Na SQ and DQF experiments were recorded at 158.660 MHz on a Varian Unity Inova 600 MHz (14.09 T) spectrometer equipped with a 5-mm Varian AutoTuneX ^{1}H/^{23}Na broadband probe. The $\pi/2$ pulse length was optimized for each sample, which ranged from 15.0 to 17.5 ms. For sodium mobility measurements, the ^{23}Na longitudinal relaxation time, T_1, was determined using the inversion-recovery (IR) pulse sequence, employing 15 inter-pulse delays from 0.125 to 2048 ms. A Carr-Purcell-Meiboom-Gill (CPMG) pulse sequence employing 31 echo times from 0.375 to 1536 ms, and an echo time of 200 μs was used to determine the ^{23}Na transverse

relaxation time, T_2, for the samples. For sodium binding measurements, DQF spectra were acquired at the optimum tau value, which was determined by collecting a spectrum of for 31 τ values ranging from 100 μs to 40 ms, at δ = 10 μs, and selecting the tau value with the largest peak area. All experiments (sodium mobility and sodium binding) were performed with a delay between scans (repetition time) of 200 ms. All acquisitions for SQ T_1 and T_2 and DQF experiments were recorded with an identical number of scans (1024), recycle delays (200 ms), and receiver gains. All experiments were conducted at room temperature (between 21.8 and 22.2 °C). Peak areas were calculated using Microsoft Excel 2010 (Microsoft Corporation, Redmond, WA, USA), applying the trapezoid rule. For the full-fat values, standard deviations ranged from ± 0.078 to 0.537 ms for T_1 and ± 0.078 to 0.134 ms for T_2. For the reduced-fat values, standard deviations ranged from ± 0.028 to 1.028 ms for T_1 and ± 0.163 to 1.499 ms for T_2. For sodium binding, the standard deviations of A_{DQ}/A_{SQ} for the reduced-fat formulation ranged from ± 0.0000225 to 0.00137 ms.

3.3.2 Viscosity Measurements

Viscosity measurements of four full-fat emulsion concentrations (7, 130, 265, 460 mg added Na/serving) and four reduced-fat emulsions concentrations (7, 140, 280, 480 mg added Na/serving) were collected using a rheometer (Model RFS-III, Rheometric Scientific, Piscataway, New Jersey) at shear rates of 10, 50, and 100 s^{-1}, to model representative in-mouth conditions (Payne and others 2010). Samples were measured at 25 ºC, and 3 measurements were obtained for each sample. Samples were tested in triplicate. The LSD statistical test was performed using the proc GLM function in Statistical Analysis Systems Program (SAS Version 9.4, SAS Inst. Inc., Cary, N.C.), at alpha = 0.05, to determine if there were significant differences

in viscosity among each of the samples. Standard deviations ranged from ± 0.28 to 9.6 cP for full-fat viscosity values and ± 0.12 to 4.9 cP for reduced-fat viscosity values.

3.3.3 pH Measurements

The pH values of four full-fat emulsion concentrations (7, 130, 265, 460 mg added Na/serving) and four reduced-fat emulsions concentrations (7, 140, 280, 480 mg added Na/serving) were measured using a pH meter (Orion VersaStar, Thermo Scientific, Waltham, MA, USA). Samples were measured at 25 ºC, and 3 measurements were obtained for each sample. The LSD statistical test was performed using the proc GLM function in Statistical Analysis Systems Program (SAS Version 9.4, SAS Inst. Inc., Cary, N.C.), at alpha = 0.05, to determine if there were significant differences in pH between each of the samples. Standard deviations ranged from ± 0.02 to 0.06 for full-fat pH values and ± 0.006 to 0.06 for reduced-fat pH values.

3.4 Results and Discussion

3.4.1 ^{23}Na NMR Results

3.4.1.1 T_1 and T_2 relaxation times

^{23}Na T_1 and T_2 SQ relaxation times were measured in the full-fat and reduced-fat model emulsion systems at added sodium levels ranging from 0 mg/serving to 480 mg/serving, and are plotted in Figure 3.1 (full-fat) and Figure 3.2 (reduced-fat). T_1 and T_2 were collected using the SQ method, and thus represent the mobility of the total sodium ion population, which is the weighted average of free and bound sodium ions in fast exchange between the two environments (Gobet and others 2009).

It appears that for both formulations, T_1 and T_2 increase at similar rates until about 230 mg added Na/serving for the full-fat, and 260 mg added Na/serving for the reduced-fat, when the

curves begin to level off and remain relatively constant. The increase in T_1 and T_2 indicates an increase in sodium ion mobility, until T_1 and T_2 remain constant, which indicates than equilibrium has been established between the free and bound sodium ions populations.

Similar trends for ^{23}Na NMR T_2 values were found previously in literature for xanthan/water systems. It was shown that for 100 mg/100 mL xanthan gum solutions, T_2 values increased initially as added sodium concentration increased, then leveled off at around 150 mg added NaCl/100 mL gum solution (Rosett and others 1995). Additionally, in a soup broth/xanthan solution, T_2 relaxation rates stayed constant from about 75 to 100 mg Na/240 mL serving, then increased until around 150 mg Na/240mL serving, then remained relatively constant until an added concentration of 500 mg Na/240 mL serving, which was the highest concentration tested (Rosett and others 1996). Similar trends for T_1 were found by Gobet and others (2009) for an iota-carrageenan gel system, in which T_1 values increased with increasing sodium concentration, until the added sodium concentration reached above 0.4 M (equivalent to 2.36 mg Na/30 g serving) and the T_1 values remained constant. T_1 for the literature carrageenan sample leveled off at around 48 ms, while both the full-fat and reduced-fat emulsions herein leveled off at around 45 ms, indicating the sodium ions have similar average mobilities. For the emulsion samples, relaxation times (T_1 and T_2) are similar for a given sodium concentration between the full-fat and the reduced-fat formulations, indicating that fat concentration does not greatly affect the total sodium ion mobility.

3.4.1.2 Relative quantification of bound sodium

The ratios of the areas of the bound sodium (DQF) to total sodium (SQ) are plotted as a function of the added concentrations of sodium in Figure 3.3. The plots are expanded in Figures 3.4 (full-fat) and 3.5 (reduced-fat) by eliminating the 0 mg added Na/serving, in order for trends in the data to be seen more clearly. At 0 mg added sodium/serving, there were DQF peaks

observed corresponding to the population of bound sodium, due to the sodium endogenous in the xanthan gum.

For the full-fat formulation (Figure 3.4), the plot can be divided into three regions. In the first and third regions (7 to 65 mg of added Na/serving and 200 to 460 mg added Na/serving), the ratio of bound/total sodium is constant; therefore, as the amount of total sodium increases, the amount of bound sodium also increases. In region 2 (100 to 200 mg added NaCl/serving), the ratio of bound/total sodium decreases, indicating the amount of bound sodium either did not increase proportionally to the amount of total sodium added, remained constant, or decreased. For the reduced-fat formulation (Figure 3.5), the trend is slightly less obvious. It seems as if from 0 to 410 mg of added Na/serving, the ratio of bound to total sodium decreases. From 410 to 480 mg of added sodium per serving, the ratio appears to remain constant. However, it is difficult to make conclusions about the data due to the high degree of variability, especially for the reduced-fat samples in the range of 210 to 280 mg added Na/serving.

In the literature, sodium binding has been investigated in different systems with varying results. In a 1% iota-carrageenan gel system, the ratio of bound to total sodium (A_{DQ}/A_{SQ}) increased from 0.05 to 0.15 M added sodium, then decreased as the binding sites became saturated (Gobet and others 2009). For a model cheese system where a low sodium cheese and a high sodium cheese were compared, other factors remaining constant, the percentage of bound sodium was slightly lower for the higher sodium cheese compared to the lower sodium cheese (12.2% versus 14.0%, respectively) (Gobet and others 2010). In a separate model cheese system, where lipid/protein ratio and sodium level were varied, there were no significant differences in sodium binding between any of the samples, indicating that the lipid/protein ratio and the salt content do did not affect the bound sodium fraction in that system (Boisard and others 2013).

No obvious correlations were observed between sodium mobility and sodium binding data. T_1 and T_2 values begin to remain constant after 230/265 mg added sodium per serving is added, respectively, but at those concentrations, A_{DQ}/A_{SQ} is constant for the full-fat formulation, but decreasing for the reduced-fat formulation. Therefore, there does not appear to be a relationship between sodium binding and total sodium mobility in this system.

3.4.2 Viscosity Results

Average viscosity values for four full-fat emulsion concentrations (7, 130, 265, 460 mg added Na/serving) and four reduced-fat emulsions concentrations (7, 140, 280, 480 mg added Na/serving), plotted at 3 shear rates (10, 50, and 100 s^{-1}) , are shown in Tables 3.7 (full-fat) and 3.8 (reduced-fat). The data shows that viscosity decreases with increasing shear rate, which is expected for a shear-thinning fluid, such as xanthan gum, and can be described by the power law equation (Pastor and others 1994):

$$\eta(\gamma) = K\gamma^{-n} \quad (1)$$

where $\eta(\gamma)$ is the viscosity, γ is the shear rate, K is the consistency index, and n is the flow behavior index.

The viscosity data also shows differing trends between the full-fat and reduced-fat emulsions. For the full-fat formulation, the viscosity increased as sodium concentration increased from 5 mg added Na/serving until 130 mg added Na/serving, then decreased from 130 to 460 mg added Na/serving. For the reduced-fat formulation, the viscosity increased from 5 mg added Na/serving to 280 mg added sodium per serving, then decreased from 280 to 480 mg added sodium per serving. The differences in viscosity trends could be due to a higher concentration of xanthan gum in the aqueous phase of the full-fat formulations compared to the reduced-fat formulations. Both formulations contain 0.8% xanthan gum (w/w), but there is a higher

concentration of water in the reduced-fat version than the full-fat version to compensate for less oil. For samples at the lowest two sodium concentrations, the viscosity of the reduced-fat formulation is statistically lower than the viscosity of the full-fat formulation. However, for the higher two concentrations, the reduced-fat formulation has a higher viscosity than the full-fat equivalents. Therefore, there appears to be an additional thickening effect due to the sodium interaction with the xanthan gum. Above the critical concentration of xanthan (2000 mg/L), an increase in viscosity with an increase in salt concentration has been attributed to an increased interaction between polymer molecules (Garcia-Ochoa and others, 2000).

The effect of salt on the viscosity of xanthan gum solutions was further explained by Zhong and others (2013). Xanthan gum is comprised of pentasaccharide repeat units, which consist of glucose, mannose, and glucuronic acid in the molar ratio 2:2:1, respectively (Garcia-Ochoa and others, 2000). It is believed that xanthan gum exists in one of two conformational states. In the ordered conformation, side chains are folded in and associated with the backbone, forming a helix. In a disordered, or extended, conformation, side chains extend away from the backbone, and the molecule occupies a larger hydrodynamic volume due to strong repulsions of like charges along the polyelectrolyte backbone. It has been shown that in solutions of low concentrations of xanthan gum solutions (less than 2000 mg/L), the negative charges on the xanthan gum are neutralized by the addition of sodium cations, which causes the elongated molecules to form helices. Since the helices take up a smaller volume than the elongated chains, the viscosity of the solution decreases as sodium concentration increases at low polymer concentration. However, when the concentration of xanthan gum is greater than the critical concentration (greater than 2000 mg/L), as is the case with the emulsions studied herein, the viscosity increases with increasing sodium concentration. Because there are more polymer

molecules, the intermolecular forces between the molecules increases, which has a greater effect on viscosity than the decrease in volume due to the transition from chains to helices. It is also hypothesized that an increase in sodium induces ion bridging between polymer chains, which would lead to as stiffer network, and thus an increase in viscosity (Wyatt and others 2010).

The differences in viscosity trends could be due to a higher concentration of xanthan gum in the aqueous phase of the full-fat formulations compared to the reduced-fat formulations. However, it is not clear as to why the viscosity begins to decrease after a certain concentration (130 mg added sodium/serving for the full-fat formulation and 280 mg of added sodium/serving for the reduced-fat formulation) of sodium ions have been added. Therefore, more research needs to be conducted in order to fully investigate the reasoning for decreasing viscosity of the emulsion system as additional sodium is added, at high concentrations of xanthan gum.

3.4.3 pH Results

Average pH values for four full-fat emulsion concentrations (7, 130, 265, 460 mg added Na/serving) and four reduced-fat emulsions concentrations (7, 140, 280, 480 mg added Na/serving) are shown in Table 3.6.

It was investigated whether the pH data may be helpful in explaining the sodium binding results. In the emulsion systems, the sodium ions are capable of binding to negatively charged carboxyl groups on xanthan gum. Xanthan gum is a polysaccharide comprised of glucose, mannose, and glucuronic acid in pentasaccharide repeat units. For every repeat unit, there are two carboxyl groups, which can be either protonated or unprotonated. If the pH of the solution is less than the pK_a of the xanthan gum carboxyl group, then the protonated form dominates. If the pH of the solution is greater than the pK_a of the carboxyl group on the xanthan gum, then the unprotonated, negatively charged form dominates. The pK_a of xanthan gum has been reported to

be between 3.1 and 3.5 (Oprea and others 2013, Desplanques and others 2014). Therefore, because the pH of the solutions ranged from 4.45 to 5.02, the unprotonated form of the carboxyl group dominates in the emulsion system. Since the pH and pK_a are known, the specific ratio of unprotonated to protonated groups can be calculated using the Henderson-Hasselbalch equation (Equation 18):

$$pH = pK_a + log_{10}(\frac{[COO^-]}{[COOH]}) \quad (18)$$

For the full-fat formulations with 7 mg, 130 mg and 265 mg of added sodium per serving, the ratios of [COO^-] to [COOH] were calculated using the pH values at the respective sodium concentrations, and found to be 50.1, 20.0, and 17.4, respectively. For the reduced-fat formulations with 7 mg, 140 mg, 280 mg, and 480 mg of added sodium per serving, the ratios of [COO^-] to [COOH] were calculated to be 50.1, 21.9, 22.4, and 14.0, respectively. Because the pH, and therefore the number of binding sites, is approximately equal between the full-fat and reduced-fat formulations for a given concentration, it does not appear that pH correlates with sodium binding. In addition, xanthan gum is 90% deprotonated at pH 4.25, and is 99% deprotonated at pH 5.30, so in the pH range of the emulsions, the unprotonated form dominates. Previous literature has shown that in a 2.5% milk protein matrix, percentage of bound sodium decreases significantly as pH decreases; however, with 9% milk protein, there were no significant differences in protein binding as pH decreased (Mosca and others 2015).

3.5 Conclusions

These results show that sodium mobility, sodium binding, and viscosity are influenced by increasing concentration of sodium ions in full-fat and reduced-fat model emulsion systems. Sodium mobility increased as sodium concentration increased, then leveled off at similar concentrations for full-fat and reduced-fat emulsion systems. Viscosity increased, then decreased

as sodium concentration increased for both reduced-fat and low-fat emulsion systems, but the concentration at which the emulsions decreased differed between the two emulsions. The pH did not seem to have an impact on sodium ion binding trends. It has been suggested that viscosity has a larger effect on salty perception than sodium ionic binding and mobility (Mosca and others 2015), so future studies should be conducted to investigate the impact of viscosity and sodium binding on salty taste of the full-fat and reduced-fat model emulsion systems.

3.6 References

Boisard L, Andriot I, Arnould C, Achilleos C, Salles C, Guichard E. 2013. Structure and composition of model cheeses influence sodium NMR mobility, kinetics of sodium release and sodium partition coefficients. Food Chemistry 136:1070-1077.

Cox GO and Lee SY. 2010. Unpublished data. University of Illinois at Urbana-Champaign. Urbana, IL.

Desplanques S, Grisel M, Malhiac C, Renou F. 2014. Stabilizing effect of acacia gum on the xanthan helical conformation in aqueous solution. Food Hydrocolloids 35:181-188.

[FDA] U.S. Food and Drug Administration. 2013. Guidance for Industry: A Food Labeling Guide (9. Appendix A: Definitions of Nutrient Content Claims). Silver Spring, MD: U.S. Food and Drug Administration. Available from: www.fda.gov. Accessed May 1, 2015.

Garcia-Ochoa F, Santos VE, Casas E, Gomez E. 2000. Xanthan gum: production, recovery, and properties. Biotechnology Advances 18:549-579.

Gobet M, Mouaddab M, Cayot N, Bonny J-M, Guichard E, Le Quere J-L, Moreau C, Foucat L. 2009. The effect of salt content on the structure of iota-carrageenan systems: ^{23}Na DQF NMR and rheological studies. Magnetic Resonance in Chemistry 47:307-312.

Gobet M, Rondeau-Mouro C, Buchin S, Le Quere J-L, Guichard E, Foucat L, Moreau C. 2010. Distribution and mobility of phosphates and sodium ions in cheese by solid-state ^{31}P and double-quantum filtered ^{23}Na NMR spectroscopy. Magnetic Resonance in Chemistry 48:297-303.

Kim MK, Lopetcharat K, Gerard PD, Drake MA. 2012. Consumer awareness of salt and sodium reduction and sodium labeling. Journal of Food Science 77(9):S307-13.

Mosca AC, Andriot I, Guichard E, Christian S. 2015. Binding of Na^+ ions to proteins: Effect on taste perception. Food Hydrocolloids 51:33-40.

Oprea AM, Nistor MT, Profire L, Popa MI, Lupusoru CE, Vasile C. 2013. Evaluation of the controlled release ability of Theophylline from Xanthan/Chondroitin sulfate hydrogels. Journal of Biomaterials and Nanotechnology 4:123-131.

Pastor MV, Costell E, Izquierdo L, Duran L. 1994. Effects of concentration, pH and salt content on flow characteristics of xanthan gum solutions. Food Hydrocolloids 8:265-275.

Rosett TR, Wu Z, Schmidt SJ, Ennis DM, Klein BP. 1995. KCl, $CaCl_2$, Na^+ binding, and salt taste of gum systems. Journal of Food Science 60(4):849-853.

Rosett TR, Kendregan SL, Gao Y, Schmidt SJ, Klein BP. 1996. Thickening agents effects on sodium binding and other taste qualities of soup systems. Journal of Food Science 61(5):1099-1104.

United States Department of Agriculture. 2010. Dietary Guidelines for Americans. www.dietaryguidelines.gov

U.S. Department of Agriculture, Agricultural Research Service and U.S. Department of Health and Human Services, Centers for Disease Control and Prevention. What We Eat In America, NHANES 2005–2006. http://www.ars.usda.gov/Services/docs.htm?docid=13793. Accessed April 28, 2015.

Wyatt NB, Gunther CM, Liberatore MW. 2011. Increasing viscosity in entangled polyelectrolyte solutions by the addition of salt. Polymer 52:2437-2444.

Zhong L, Oostrom M, Truex MJ, Vermeul VR, Szecsody JE. 2013. Rheological behavior of xanthan gum solution related to shear thinning fluid delivery for subsurface remediation. Journal of Hazardous Materials 244:160-170.

3.7 Tables and Figures

Table 3.1. Formulations for Full-Fat Emulsions (%w/w).

Rounded Concentration (mg added Na/30 gram serving)	0	7	65	100	130	150	170	200	230	265	300	350	395	460
Oil (%w/w)	39.82	39.81	39.74	39.70	39.66	39.63	39.61	39.59	39.53	39.50	39.45	39.39	39.34	39.26
Water (%w/w)	58.45	58.41	57.98	57.74	57.50	57.36	57.22	57.03	56.80	56.55	56.27	55.96	55.62	55.16
NaCl (%w/w)	0.00	0.06	0.56	0.84	1.12	1.29	1.46	1.67	1.95	2.24	2.56	2.94	3.34	3.87
Xanthan gum (%w/w)	1.06	1.06	1.06	1.06	1.06	1.06	1.06	1.06	1.05	1.05	1.05	1.05	1.05	1.05
Soy lecithin (%w/w)	0.66	0.66	0.66	0.66	0.66	0.66	0.66	0.66	0.66	0.66	0.66	0.66	0.66	0.65

Table 3.2. Formulations for Reduced-Fat Emulsions (%w/w)

Rounded Concentration (mg added Na/30 gram serving)	0	7	35	70	140	210	220	235	250	260	280	345	410	480
Oil (%w/w)	27.88	27.87	27.84	27.81	27.76	27.70	27.69	27.68	27.66	27.65	27.64	27.58	27.53	27.47
Water (%w/w)	70.31	70.26	70.05	69.79	69.26	68.74	68.64	68.53	68.43	68.32	68.21	67.70	67.19	66.68
NaCl (%w/w)	0.00	0.06	0.30	0.59	1.18	1.76	1.87	1.99	2.10	2.23	2.35	2.92	3.50	4.07
Xanthan gum (%w/w)	1.12	1.11	1.11	1.11	1.11	1.11	1.11	1.11	1.11	1.11	1.11	1.10	1.10	1.10
Soy lecithin (w/w)	0.70	0.70	0.70	0.70	0.69	0.69	0.69	0.69	0.69	0.69	0.69	0.69	0.69	0.69

Table 3.3. Exact and Rounded Concentrations of Added Sodium in Full-Fat Emulsion Systems (mg added Na/30 gram serving).

Exact Sodium Concentration	0.00	6.66	66.44	98.91	132.61	152.01	171.74	197.25	230.66	264.15	302.64	347.31	394.59	456.93
Rounded Sodium Concentration	0	7	65	100	130	150	170	200	230	265	300	350	395	460

Table 3.4. Exact and Rounded Concentrations of Added Sodium in Reduced-Fat Emulsion Systems (mg added Na/30 gram serving).

Exact Sodium Concentration	0.00	6.99	34.91	69.75	139.22	207.57	220.56	235.16	248.12	262.70	277.26	345.04	412.54	479.76
Rounded Sodium Concentration	0	7	35	70	140	210	220	235	250	260	280	345	410	480

Table 3.5. Sodium amounts per serving in six commercial ranch dressings of full-fat, light, and fat-free varieties

Ranch Dressing (Brand and Fat Level)	Sodium amount (mg) per serving
Kraft Original	260 mg Na/28 g serving
Hidden Valley Original	260 mg Na/30 mL serving
Kraft Lite	350 mg Na/32 g serving
Hidden Valley Light	260 mg Na/30 mL serving
Kraft Fat-Free	220 mg Na/34 g serving
Hidden Valley Fat-Free	310 mg Na/32 g serving

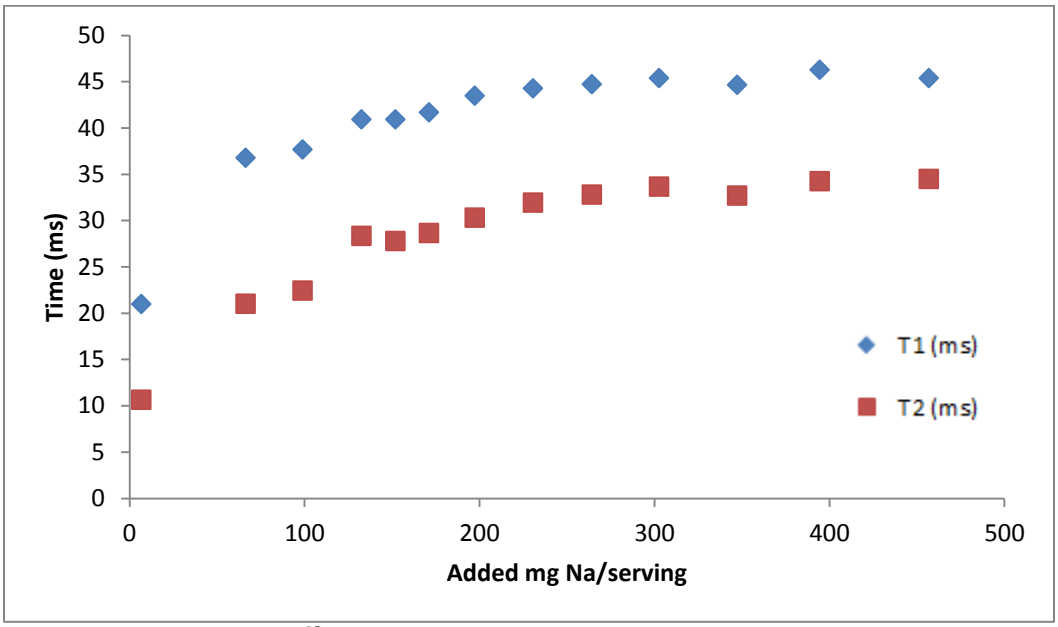

Figure 3.1. Average NMR ^{23}Na T_1 and T_2 relaxation times for full-fat model emulsions, with added sodium levels ranging from 7 mg/serving to 460 mg/serving.

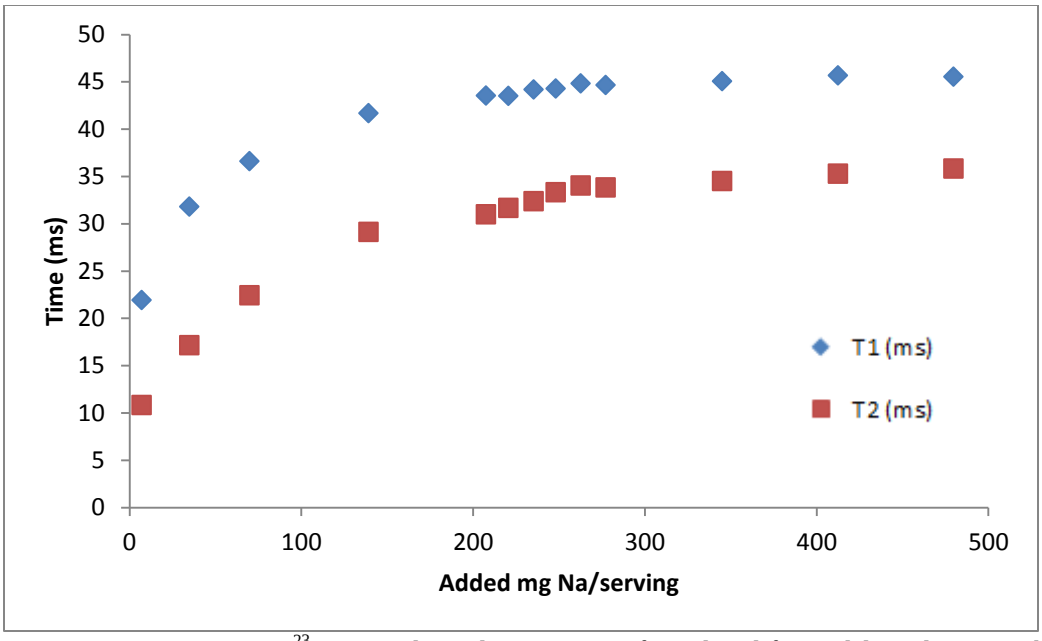

Figure 3.2. Average NMR ^{23}Na T_1 and T_2 relaxation times for reduced-fat model emulsions, with added sodium levels ranging from 7 mg/serving to 480 mg/serving.

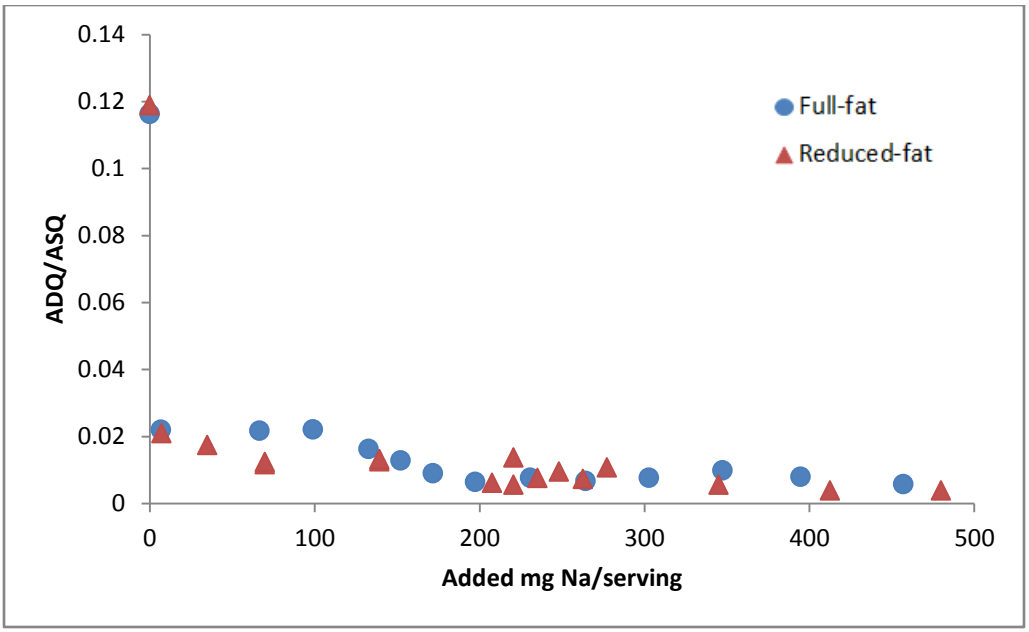

Figure 3.3. Ratio of the average areas of bound peaks (ADQ) to average areas of total sodium peaks (ASQ) in full-fat and reduced-fat emulsion systems from 0 to 480 mg added Na/serving.

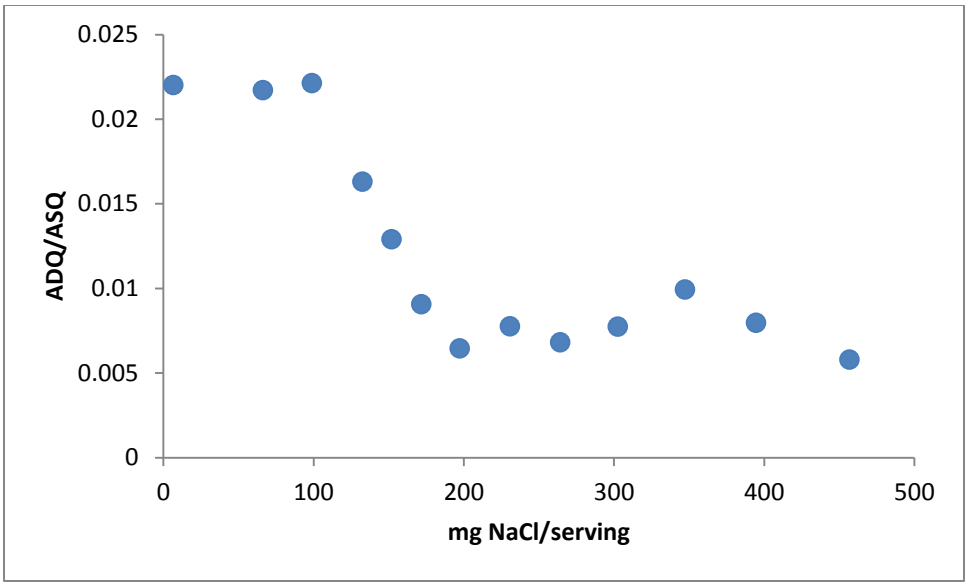

Figure 3.4. Ratio of the average areas of bound peaks (ADQ) to average areas of total sodium peaks (ASQ) in full-fat emulsion systems from 7 to 460 mg Na/serving.

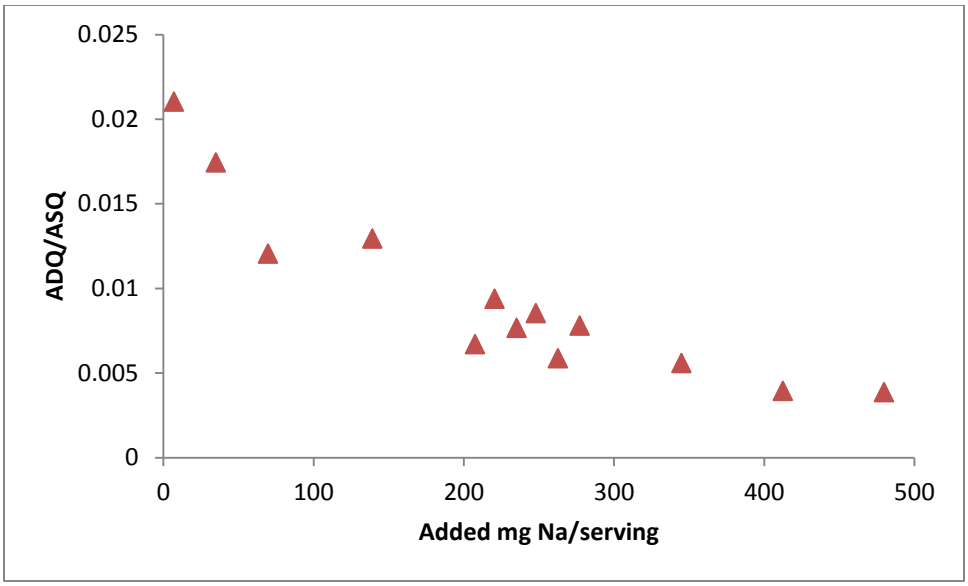

Figure 3.5. Ratio of the average areas of bound peaks (ADQ) to average areas of total sodium peaks (ASQ) in reduced-fat emulsion systems from 7 to 480 mg added Na/serving.

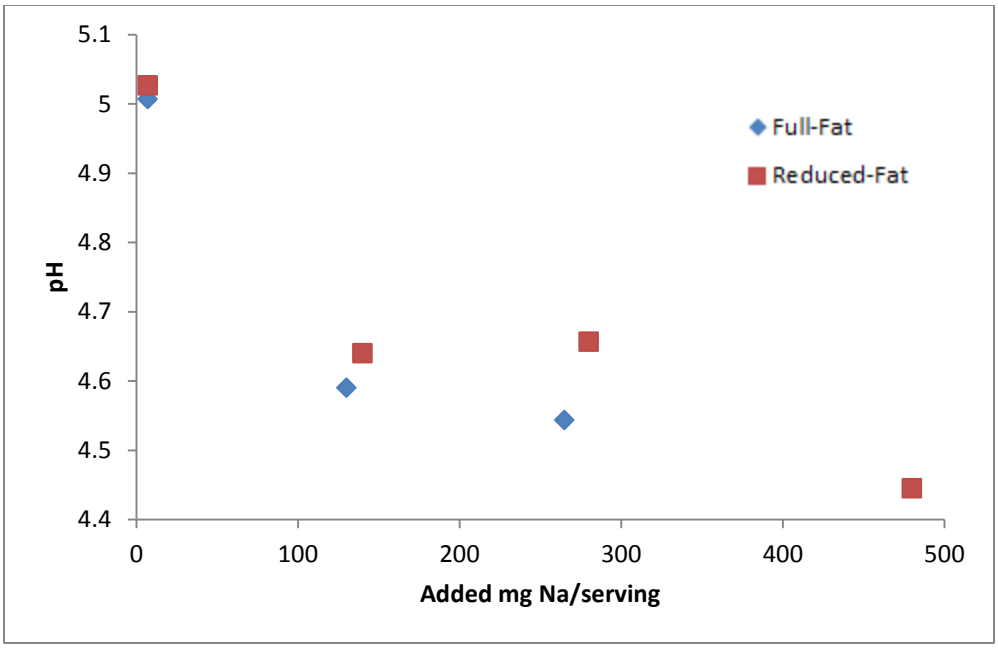

Figure 3.6. Average pH data for full-fat and reduced fat model emulsions, with added sodium levels ranging from 7 mg/serving to 480 mg/serving.

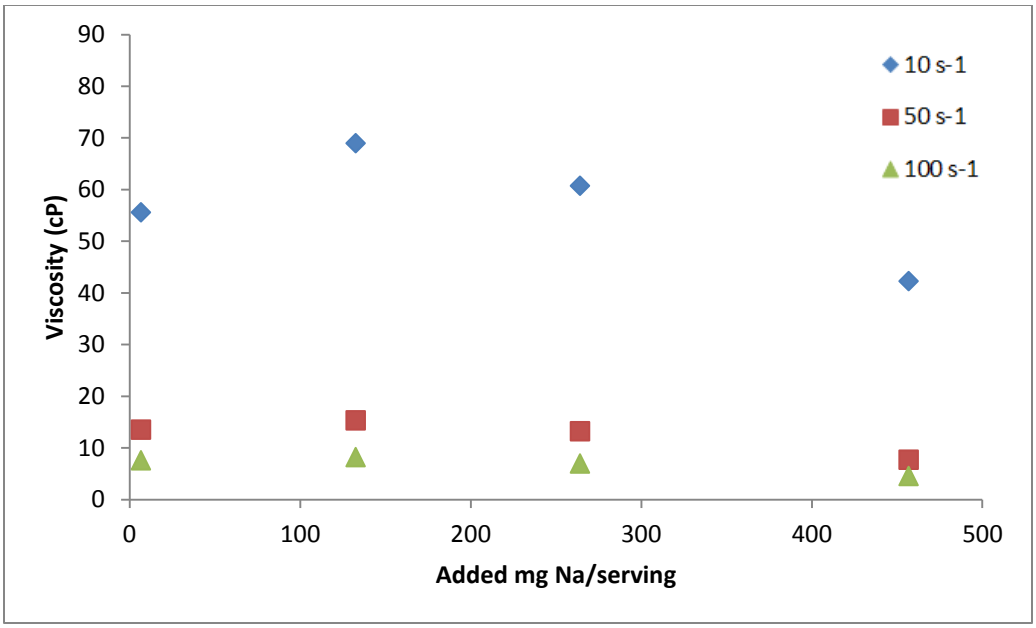

Figure 3.7. Average viscosity data for full-fat model emulsions, at three different shear rates, with added sodium levels ranging from 7 mg/serving to 460 mg/serving.

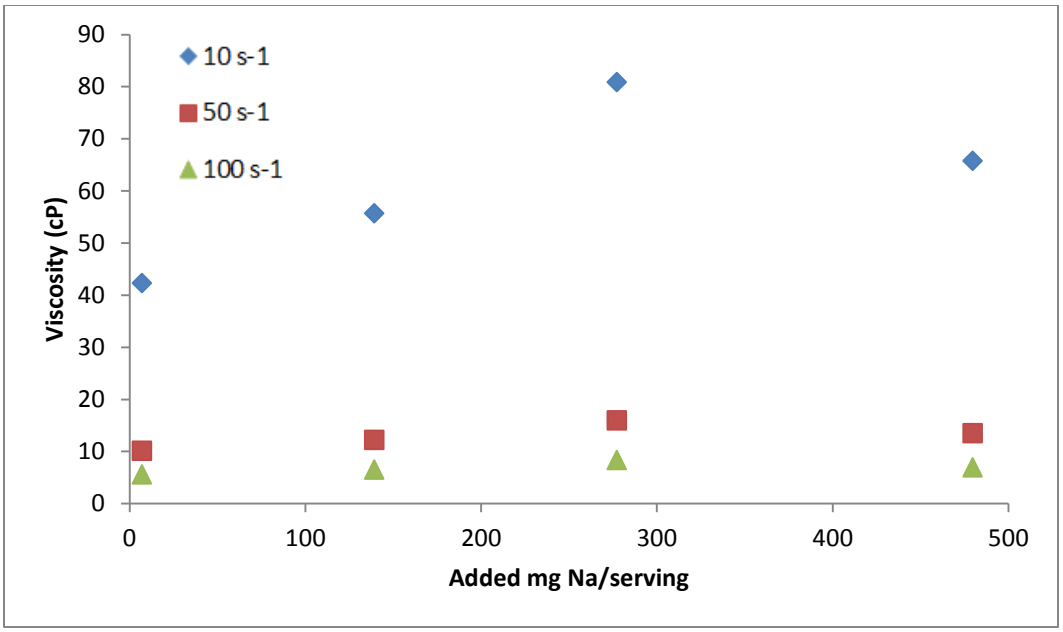

Figure 3.8. Average viscosity data for reduced-fat model emulsions, at three different shear rates, with added sodium levels ranging from 7 mg/serving to 480 mg/serving.

Appendix A: ^{23}Na NMR Protocol for Iota-Carrageenan and Emulsion Samples

‘_____’ = type and hit Return on keyboard
[_____] = click button with mouse
(_____) = notes/comments about command

- Insert sample
    - Log in to ChemFOM using username and password on login computer
    - Walk back to NMR computer
    - Insert NMR tube into plastic casing
        - *Make sure sample is centered in opening (will affect tuning)
    - ‘e’ (ejects sample, shouldn’t be a sample already in there)
    - Insert NMR tube in plastic casing in NMR
    - ‘i’ (insert) (wait for click)
    - ‘logon’
    - ‘directory name’ (don’t actually type ‘directory name’ – type whatever yours actually is)
- Tune (^{1}H first, then ^{23}Na)
    - [Main Menu]
    - [Setup]
    - [Nuc, Solv]
    - [H1]
    - [D2O] (even if there isn’t D2O in sample)
    - [Acqi]
    - [Lock]
    - [Off] (because there isn’t any D2O in the sample – D2O locks the magnetic field, so if no D2O, record Z0 and turn off lock; Best to use at least 10% D2O if possible to stabilize chemical shifts; should also use at least a little H2O so can autoshim – otherwise have to shim manually)
    - [Close]
    - ‘su’
    - Follow instructions on diagram for which cables to move where
        - Disconnect 1H cable, connect end attached to NMR to PROBE TUNE INTERFACE
        - Disconnect cable connected to OUTPUT and connect to TUNE OUTPUT
        - Press + button to change channel from 0 to 1 on the TUNE INTERFACE
        - Use red tune and match knobs on NMR probe to reduce reflected power number to 0 (or at least under 5)
        - Press the – button to change channel from 1 to 0
        - Reattach cables to initial positions
        - Move cable attached to OUTPUT on left-hand side to TUNE OUTPUT
    - ‘autotune’
    - ‘Na23’
    - Hit Return key on keyboard again
    - Wait for the message in the command line of VNMR to say ‘Ok… ‘ to indicate tuning is complete

        - X-channel autotune cables will change, creating a whirring sound – watch to make sure cables don't fall out, and tell someone if they do
    - If the TUNE INTERFACE light is still on (it probably will be), push + button to change to channel 1, then push the – button to change it back to 0 (the light should go off)
    - Move cable back to original position
- To collect ^{1}H spectrum
    - 'gain='n''
    - 'ga'
    - Wait until you hear a beep, indicating the experiment has finished
    - 'wft' (weighted fourier transform)
    - 'aph' (autophase)
    - Use middle mouse key to autoscale
    - 'nl' (nearest line)
    - 'dres' (to determine linewidth at half height)
    - Record linewidth at half height
    - 'svf('_____')' (to save file)
- To collect ^{23}Na spectrum
    - 'jexp2' (jump to experiment 2)
    - [Setup]
    - [Nuc, Solv]
    - [Other]
    - 'Na23'
    - [D2O] (even if there isn't D2O in sample)
    - 'gain='n''
    - 'ga'
    - Wait for experiment to finish
    - 'aph'
    - 'gain?'
    - Note the gain value used, but subtract 4 from it for next run
    - 'gain=____' (4 minus whatever the autogain number was)
    - 'array'
    - 'pw'
    - '10'
    - '56'
    - '1'
    - 'pw[1]=15'
    - 'd1=0.2'
    - 'at=0.4'
    - 'go'
    - Wait for experiment to finish
    - 'wft'
    - 'ai'
    - 'aph'

- ‘da’
- ‘dssh’ (look where the peaks switch from negative to positive, estimate pw (closer to one with larger peak) – if all peaks are positive, re-do array with lower initial value (e.g. use 52 instead of 56))
- Record pw90 value
- ‘pw90=___/4’
- ‘pw=pw90’
- ‘gain=’n’’
- ‘go’
- Wait for experiment to finish
- ‘gain?’
- Set gain to 4 less than the auto gain value
- ‘gain=___’ (Use this value for all future experiments)
- ‘go’
- Wait for experiment to finish
- ‘wft’
- ‘nl’
- ‘dres’
- Record linewidth at half height

- To find T_1
  - ‘jexp3’
  - ‘mf(2,3)’ (Make sure gain and pw90 are the same from exp 2)
  - ‘dot1’
  - ‘0.001’
  - ‘0.5’
  - ‘1’
  - ‘gos(‘_____’) (Fill in blank with file name) (This command is go and save combined)
  - ‘wft’
  - ‘aph’
  - ‘dssh’ (should have negative peaks, then positive peaks)
  - ‘dll’
  - ‘fpdc’
  - ‘t1’ (record T2 value and error)

  OR (If you have already measured this parameter using other samples)
  - ‘jexp3’
  - [Main Menu]
  - [File] (Find a previous T1 data file, click on that file)
  - [Load]
  - ‘wft’
  - ‘pw90=____/4’ (use same value as exp 2)
  - ‘pw=pw90’
  - ‘gain=_____’ (use same value from exp 2)

- ‘gos(‘_____’) (Fill in blank with file name) (This command is go and save combined)
- ‘wft’
- ‘aph’
- ‘dssh’ (should have negative peaks, then positive peaks)
- ‘dll’
- ‘fpdc’
- ‘t1’ (record T2 value and error)

- To find T_2
  - ‘jexp4’
  - ‘mf(2,4)’ (Make sure gain and pw90 are the same from exp 2 and 3)
  - ‘doT2’
  - ‘d2=0.0002’
  - ‘nt=1’
  - ‘bt=0.000375, 0.0005, 0.0075, 0.0009, 0.0015, 0.0022, 0.003, 0.0045, 0.006, 0.008, 0.01, 0.012, 0.015, 0.018, 0.021, 0.024, 0.028, 0.032, 0.036, 0.04, 0.048, 0.058, 0.068, 0.078, 0.088, 0.096, 0.015, 0.0192, 0.0384, 0.0768, 1.536’
  - ‘gos(‘_____’)’ (put whatever you want the file name to be in the blank)
  - ‘aph’
  - ‘dssh’ (when finished – should look like decay curve)
  - ‘ds(1)’
  - [Th] (make sure line is only going through one peak)
  - ‘dll’
  - ‘fpdc’
  - ‘t2’ (record T2 value and error)

  OR (If you have already measured this parameter using other samples)
  - ‘jexp4’
  - [Main Menu]
  - [File] (Find a previous T2 data file, click on that file)
  - [Load]
  - ‘wft’
  - ‘pw90=____/4’ (use same value as exp 2 and 3)
  - ‘pw=pw90’
  - ‘gain=_____’ (use same value from exp 2 and 3)
  - ‘gos(‘_____’) (Fill in blank with desired file name) (This command is go and save combined)
  - ‘aph’
  - ‘dssh’ (when finished – should look like decay curve)
  - ‘ds(1)’
  - [Th] (make sure line is only going through one peak)
  - ‘dll’
  - ‘fpdc’
  - ‘t2’ (record T2 value and error)
- To array tau (in order to calculate tau opt)

- ‘jexp5’
- ‘mf(2,5)’
- ‘dqft2’
- ‘delta=10’
- ‘array’
- ‘tau’
- ‘25’ (or however many tau values you want to array)
- ‘0.0001’ (starting value)
- ‘0.002’ (increment)
- ‘il=’y’’
- ‘nt=256’
- ‘gos(‘_____’) (insert desired file name into blank)

OR (If you have already measured this parameter using other samples)

- ‘jexp5’
- [Main Menu]
- [File] (Find a previous T2 data file, click on that file)
- [Load]
- ‘wft’
- ‘pw90=____/4’ (use same value as exp 2 and 3)
- ‘pw=pw90’
- ‘gain=_____’ (use same value from exp 2 and 3)
- ‘gos(‘_____’) (insert desired file name into blank)

- Set up 3 replicates of sodium spectrum (while tau opt is running)
  - ‘jexp2’
  - ‘nt=1024’
  - ‘gos(‘_____’) (fill in blank with desired file name)
  - ‘jexp6’
  - ‘mf(2,6)’
  - ‘gos(‘_____’)’
  - ‘jexp7’
  - ‘mf(2,7)’
  - ‘gos(‘_____’)’
- Set up 3 replicates for dqft2 peak (While waiting for tau array to finish, you can look at the tau array and estimate the optimum tau value – look at highest peak and up to two values around it that could also be the optimum)
  - ‘jexp5’
  - ‘wft’
  - ‘dssh’
  - ‘da’
  - ‘dssl’ (once all peaks are collected, look at which peak is highest)
  - ‘jexp8’
  - ‘mf(5,8)’
  - ‘tau=_____, _____, _____’
  - ‘nt=1024’ (make sure this matches the nt value for the sodium spectra)

    - ‘il=’n’’
    - ‘gos(‘_____’)’
    - ‘jexp9’
    - ‘mf(8,9)’
    - ‘gos(‘_____’)’
    - ‘jexp10’
    - ‘mf(8,10)’
    - ‘gos(‘_____’)’
- Once all experiments are complete:
    - ‘e’ (ejects sample)
    - ‘i’ (don’t have to insert another sample)
    - ‘logoff’
    - Log off of ChemFOM computer

Appendix B: Viscosity Testing Protocol

- Before unlocking, make sure you have pressure on
    - Pressure (red tube) – attach to red pressure unit
    - Attach red tube to any of 3 openings (lift up gold covering on pressure unit and then push up into opening, covering should be down)
        - *Make sure there are no other attachments to pressure unit and check to make sure no one else is using pressure/make sure equipment connected to pressure is turned off
    - Turn pressure on (blue handle counter clockwise)
    - Check to see it's 80 lb/in^2 at yellow tape
    - Check side pressure readings on rheometer (35/60/40)
    - Plug in black cord into outlet 208VIPH (can put cable on floor when using, but put back on bench when done; can be little gap when plug in to outlet)
    - Turn on machine (button on back)
- Switch to unlock (make sure there's enough pressure)
- Get probe – in 1st drawer (401687.901) (Geom 50mm Cross Hatch Plt 316SST ARES, bottom left drawer)
- Push probe in gently, turn screws to tighten evenly on both side (check with machine readings as well to see if force is equilibrated) (fit probe into cavity, screw R&L at same time)
- Computer – Turn on; login info on paper towel (FSHN-ylee; AESB267)
    - Open TA Orchestrator (Note: Error message may appear during this process which is okay)
    - Control – Set Test Conditions - 25°C
    - Control – Instrument Control Panel
        - 25°C
        - Peltier
        - Environmental Controller – ON
        - Motor Power – ON (bottom plate will rotate quickly)
    - Control – Set End of Test Conditions
        - Turn Off Temp Controller – NO
        - Set End of Test Temp – YES (25°)
        - Turn Off Motor – NO
        - Turn Hold On - NO
    - Control – Motor Mode: Steady
    - Control – Gap Control Panel
        - Torque (force in horizontal direction – should be 0) – offset torque to zero
        - Force (vertical pressing force) – offset force to zero
        - Manually lower probe (press 2 down arrow buttons together) till probe almost touches silver surface
        - Max allowed force don't change
        - Hit zero fixture (DO NOT TOUCH RHEOMETER DURING THIS PROCESS)

Appendix B (cont.)

- Then exit

- Set Water Bath
  - Make sure black ropes are connected to rheometer (if not connect them)
  - Make sure water is in water bath – if not fill with deionized water
  - Turn on water bath (in back), turn power button on
  - Set temperature (press button so that it won't flash)
  - Press gray button for 10 s to reset, if necessary
- Control – Edit/Start Test
  - Test Setup
  - Predefined Test Setup – use Stored Test Setup if you have already saved test conditions (Browse – my computer – TA – user – viscosity salad dressings test)
  - Thixotropic Loop (shear thinning high to low speed, low to high speed)
- Edit Test
  - Temp - 25°C
  - Sampling Mode – Log
  - Points Per Zone – 200
  - Final Sheer Rate – 150, 0, 0, 0
  - Zone time – 150, 30, 0, 0
  - Direction – Clockwise
  - Options – Analog Data Input – OK
  - End of Test (same as other conditions)
  - OK
  - Save As – Viscosity Salad Dressings (or whatever)
  - Sample Geometry – Predefined Geometry – Parallel Plate Geometry
  - Folder – your name
  - Title – Sample 1, Rep 1(4)
- Load Sample
  - Lift up probe by using 2 up arrows on side
  - Put quarter size amount gently onto rheometer – use spatula
  - Manually lower probe until almost hit sample
  - Control – Gap Control Panel – Command Gap 1.05 – Set Gap
  - Using scraper, scrape excess sample residue off of silver portion of rheomter
  - Cover sample with covering
  - Change Command Gap to 1 – Set Gap
  - Wait 5 minutes
  - Click Green Arrow button, Name the sample, Click Begin Test, Motor On when motor message appears
- During/After Test (Start button will appear to indicate it is finished)
  - Right click Plot Setup
  - Layout
  - Click *n* (viscosity)

        - Add
        - Ok
        - Press pic with overlapping curves
        - Copy data and paste into Excel Spreadsheet – save on flash drive
- To repeat measurement:
    - Remove casing
    - Use 2 up arrows to lift up probe, clean off emulsion with wet and dry kim wipes
    - Recalibrate: Control – Gap Control Panel
        - Torque (force in horizontal direction – should be 0) – offset torque to zero
        - Force (vertical pressing force) – offset force to zero
    - Load Sample
        - Lift up probe by using 2 up arrows on side
        - Put quarter size amount gently onto rheometer – use spatula
        - Manually lower probe until almost hit sample
        - Control – Gap Control Panel – Command Gap 1.05 – Set Gap
        - Using scraper, scrape excess sample residue off of silver portion of rheomter
        - Cover sample with covering
        - Change Command Gap to 1 – Set Gap
        - Wait 5 minutes
        - Click Green Arrow button, Name the sample, Click Begin Test, Motor On when motor message appears
    - During/After Test (Start button will appear to indicate it is finished)
        - Right click Plot Setup
        - Layout
        - Click *n* (viscosity)
        - Add
        - Ok
        - Press pic with overlapping curves
        - Copy data and paste into Excel Spreadsheet – save on flash drive
- Turning off the Rheometer
    - Shut down computer
    - Turn off water bath
    - Lock rheometer
    - Turn off rheometer
    - Unplug rheometer
    - Turn off pressure
    - Unplug red cord (wait for pressure to decrease a little bit)

Appendix C: Data Tables for τ^{opt} Curves

tau (s)	DQF Peak Area (a.u.)
0	0.40836
0.002	8.199176
0.004	14.9146
0.006	20.56047
0.008	24.7991
0.01	27.64295
0.012	28.99044
0.014	30.87781
0.016	32.31365
0.018	32.40656
0.02	32.00832
0.022	32.08483
0.024	32.55514
0.026	32.12644
0.028	31.33325
0.03	30.29504
0.032	28.19345
0.034	25.33492
0.036	23.05604
0.038	22.01367
0.04	20.58125
0.042	19.43814
0.044	18.77168
0.046	18.30872
0.048	17.81384
0.05	16.77559
0.052	15.42711
0.054	13.98767
0.056	11.68134
0.058	10.30278
0.06	9.075346
0.062	8.239023

Table C.1. Data from iota-carrageenan samples corresponding to Figure 2.16. The areas were measured using Microsoft Excel by using the trapezoid rule.

Appendix C (cont.)

tau (s)	DQF Peak Area (a.u.)
0	1.339698
0.001	7.947592
0.002	13.8443
0.003	18.7287
0.004	22.96683
0.005	26.2175
0.006	28.58735
0.007	30.90908
0.008	31.36243
0.008	32.14759
0.009	32.35072
0.009	32.5921
0.009	32.48722
0.009	32.65283
0.01	32.60888
0.01	32.48779
0.01	32.1726
0.01	32.33743
0.011	32.40952
0.011	32.10781
0.011	31.88186
0.012	31.47229
0.012	31.13296
0.013	29.39185
0.014	28.04695
0.016	24.55491
0.018	20.53451
0.02	17.19793
0.022	13.58006
0.024	10.52848
0.026	8.21013
0.028	6.155662
0.03	4.70548

Table C.2. Data from 250 mg Na/serving reduced-fat model emulsion samples corresponding to Figure 2.17. The areas were measured using Microsoft Excel by using the trapezoid rule.

Appendix D: T_1 and T_2 Data, Model Emulsion System

Added mg Na/serving	T_1 avg. (ms)	St. Dev. (ms)	T_2 avg. (ms)	St. Dev. (ms)
7	20.97		10.66	
65	36.77		21	
100	37.67		22.42	
130	40.92	0.0778	28.35	0.0778
150	40.93		27.78	
170	41.68		28.63	
200	43.47		30.3	
230	44.28		31.93	
265	44.72		32.78	
300	45.38		33.64	
350	44.64	0.537	32.685	0.134
395	46.27		34.26	
460	45.36		34.5	

Table D.1. Data from full-fat emulsion samples corresponding to Figure 3.1.

Appendix D (cont.)

Added mg Na/serving	T_1 avg. (ms)	St. Dev. (ms)	T_2 avg. (ms)	St. Dev. (ms)
7	21.92		10.84	
35	31.82		17.16	
70	36.595	0.176777	22.425	2.269813
140	41.685	0.572756	29.12	0.381838
210	43.55	0.59397	31	1.499066
220	43.51333	1.027732	31.67333	0.514231
235	44.19	0.876812	32.37	0.876812
250	44.3	0.028284	33.335	0.799031
260	44.83	0.042426	34.025	0.162635
280	44.64	0.19799	33.835	0.643467
345	45.06		34.5	
410	45.67		35.28	
480	45.54		35.82	

Table D.2. Data from reduced-fat emulsion samples corresponding to Figure 3.2.

Appendix E: A_{DQ}/A_{SQ} Data, Model Emulsion Systems

Added mg Na/serving	ADQ/ASQ
7	0.02202
65	0.021716
100	0.01631
130	0.006443
150	0.007746
170	0.006805
200	0.007731
230	0.009936
265	0.007956
300	0.00579
350	0.02213
395	0.01289
460	0.00905

Table E.1. Data from full-fat emulsion samples corresponding to Figure 3.3 and Figure 3.4.

Appendix E (cont.)

Added mg Na/serving	ADQ/ASQ	St. Dev.
7	0.02102	
35	0.01743	
70	0.01205	0.000625
140	0.01293	0.000467
210	0.00669	0.000768
220	0.009388	0.004069
235	0.007654	2.25E-05
250	0.008521	0.001365
260	0.00587	0.002081
280	0.007794	0.004237
345	0.005573	
410	0.003937	
480	0.003857	

Table E.2. Data from reduced-fat emulsion samples corresponding to Figure 3.3 and Figure 3.5.

Appendix F: NovaXan™ NF/FCC (Xanthan Gum) Nutritional Information, from ADM

Nutrient	Nutrient Quantity/100 grams of Ingredient
Total Calories	335.4 Kcal
Calories from Fat	0 Kcal
Calories from Saturated Fat	0 Kcal
Total Fat	<0.1 g
Saturated Fat	0.01 g
Polyunsaturated Fat	0 g
Monounsaturated Fat	0.01 g
Trans Fats	0.0 g
Cholesterol	0 mg
Sodium	2620 mg
Potassium	524 mg
Total Carbohydrate	77.2 g
Dietary Fiber	77.2 g
Soluble Fiber	75.0 g
Insoluble Fiber	2.2 g
Sugars	0 g
Sugar Alcohol	0 g
Other Carbohydrate	0 g
Protein (Kjeldahl Nitrogen analysis)	6.64 g
Vitamin A	0 IU
Vitamin C	0 mg
Calcium	16.5 mg
Iron	0.22 mg
Moisture	6.92 g
Ash	9.22 g